Common mycelial network modulates neighbour-primed plant defences against foliar pathogens by co-opting distinct inter-plant metabolic and biotic stress responses.

Zigmunds Orlovskis[1*], Ilva Nakurte[2], Ēriks Voroņins[1], Annija Kotova[1], Daniels Pugačevskis[1], Dawood Shah[1], Annija Andersone[1], Kārlis Trevors Blūms[1], Ivars Silamiķelis[1], Soon-Jae Lee[3]

[1] Latvian Biomedical Research and Study Centre, Rātsupītes iela 1k-1, Rīga, LV-1067, Latvia
[2] Institute for Environmental Solutions, "Lidlauks", Priekuļu pagasts, Cēsu novads, LV-4126, Latvia
[3] Department of Ecology and Evolution, University of Lausanne, UNIL-Sorge, CH-1015, Switzerland

***Correspondence:** zigmunds.orlovskis@biomed.lu.lv

Running head: Common Mycelial Networks Modulate Neighbour-Primed Plant Defences

Author Orchid IDs:
ZO: 0000-0001-8583-9814
IN: 0000-0001-9070-3479
EV: 0009-0004-1644-6864
AK: 0009-0005-8476-516X
DP: 0009-0002-0285-6999
AA: 0009-0009-9102-7236
KTB: 0009-0009-5290-3846
IS: 0000-0002-7932-1047
SJL: 0000-0002-7216-0236

Abstract

Arbuscular mycorrhizal fungi (AMF) are ubiquitous root symbionts that form common mycelial networks (CMN), linking multiple plants underground. CMN are hypothesized to play a role for information exchange between plants for neighbour-primed defences. However, the key transcriptomic and metabolome responses in receiver plant associated with inter-plant CMN connections remain yet to be elucidated. Additionally, the confounding effects of hyphal damage from CMN disconnection have not been clearly resolved. To uncover the contribution of CMN integrity to neighbour-primed plant defences, we used model AMF *Rhizophagus irregularis* to inter-connect two *Medicago truncatula* plants and explored the effect of sender wounding and *flg22* elicitation on receiver plants' leaf responses and pathogen tolerance. For the first time, we demonstrate that changes in receiver's biotic stress and defence signalling pathways rely on CMN-mediated inter-plant signals, not on mycelial network damage. This response was associated with distinct leaf isoprenoid production, including volatile monoterpenes and triterpene saponins. Furthermore, CMN-mediated

signals from stressed senders enhanced receiver resistance to *Fusarium sporotrichoides* whilst simultaneously increasing susceptibility to *Botrytis cinerea*. Our findings highlight the critical role of CMN in inter-plant signalling for pathogen-specific susceptibility and resistance which can be a key for understanding plant community-level defence in nature and agroecosystems.

Key words: common mycelial networks, inter-plant signals, plant defence, neighbour modulated susceptibility, systemic signals, pathogen resistance, *Medicago truncatula,* arbuscular mycorrhiza, *Rhizophagus irregularis,* RNA-seq, leaf metabolomics

Introduction

Exchanging danger signals between plants provides an effective strategy for priming the defences of receivers and preparing them for imminent pest or pathogen attacks that have already affected their neighbours. Such inter-plant communication may contribute to enhanced community-level resilience against biotic stress and presents a promising trait for future crop improvements and agricultural engineering. Upon perception of pest and pathogen elicitors such as herbivore eggs[1] or bacterial virulence proteins[2] plants are known to elevate pathogen resistance in their neighbours via airborne volatile or soil-mediated signals. Furthermore, ubiquitous plant root symbionts, such as arbuscular mycorrhizal fungi (AMF), are capable of inter-connecting root systems from multiple plant hosts, effectively forming underground common mycelial networks (CMN) which are hypothesized to function as information superhighway in transferring diverse signals from plant-to-plant in response to different sender plant stimuli[3,4]. Given that the vast majority of land plants form AMF symbiosis[5], testing this hypothesis is paramount to understanding the ecological roles and mechanisms how CMN can contribute to the health of wild plants and crops.

While a few studies[6–8] have implicated CMN for nutrient redistribution among the connected plants, functional studies on CMN-mediated inter-plant signals involved in plant defences and stress tolerance have been extremely scarce to date. Moreover, in all previous studies, which used CMN disruption[9,10] to test the hypothesis whether CMN mediates stress-induced inter-plant signals, the effect from CMN disruption was confounded by mechanical damage of the symbiotic hyphal network. Therefore, the neighbour plant responses to signals associated with disconnection of inter-plant CMN were not decoupled from potential plant responses resulting from CMN hyphal damage. Another key shortcoming of the previous studies is the lack of a control for inducible sender or donor plant signal. For example, previous studies in tomato[9] and pea[10] did not include controls for pathogen non-infected or aphid non-infested sender plants, impeding non-biased conclusions about participation of CMN in stress-inducible as opposed to constitutive inter-plant signal exchange.

In the present study, we sought to overcome the limitations by previous studies and test two working hypotheses: whether inter-plant CMN connection, firstly, contributes to distinct receiver responses to stress-induced inter-plant signals and, secondly, mediates neighbour-primed defences against plant pathogens. To decouple the effect of CMN disruption from the symbiotic hyphal network damage, we set an

experimental control where the disruption of mycorrhizal hyphal network occurs without perturbing the inter-plant CMN continuity. We used model AMF *Rhizophagus irregularis* to establish CMN between two *Medicago truncatula* plants, then subjected the leaves of signal senders to known plant defence elicitors with non-stimulated sender controls and analysed transcriptional and metabolic responses in naïve signal receiver plants. Intriguingly, we discovered CMN-connection dependent transcriptional changes in receivers, involving strong modulation of multiple plant biotic stress and defence signalling pathways. Moreover, leaf isoprenoid, especially monoterpene and triterpene saponin, production was elevated in receivers with the intact inter-plant CMN compared to the cut CMN independently from hyphal damage, strongly supporting our first hypothesis. Surprisingly, after the elicitation of sender plants, CMN-connected receiver plants exhibited heightened susceptibility to the fungal pathogen *Botrytis cinerea*, while simultaneously showing increased resistance to *Fusarium sporotrichoides*. This finding aligns with our second hypothesis whilst revealing previously undocumented species-specific effects in neighbour-modulated pathogen susceptibility within CMN-linked plant systems.

Results

Wounding combined with flg22 induces local leaf responses and systemic acquired resistance to Botrytis cinerea

To test the responses of signal receivers to sender stimuli, we first wished to identify stimuli that would induce leaf responses in the signal senders themselves. To this end we subjected leaves to mechanical wounding by forceps as well as applied a well-known plant immunity elicitor - bacterial flagellin (*flg22*). Since *flg22* and wounding have been well documented to induce different defence responses in leaves of a model plant *Arabidopsis thaliana*[11] and are required in combination to activate defence in plant roots[12], we also decided to test the combination of both wounding and *flg22*. This would mimic a natural scenario where bacterial infections follow mechanical plant damage by leaf herbivores, for example. Additionally, we also infiltrated a mixture of live plant pathogenic bacteria with a broad host range (*Pantotea aglomerans, Pseudomonas syringae pv. tomato, Erwinia rhapontici, Dickeya chrysanthemi*) to test for their ability to trigger local responses in the infected leaves. We selected a range of known plant immunity genes as potential markers for local leaf responses, designed primers for their homologs in *Medicago* truncatula and performed rt-qPCR at 2h, 4h and 6h following the application of the abovementioned stimuli. Leaves infiltrated with *flg22* and leaves treated with the combination wounding and *flg22* (*WF*) displayed strong induction of *MtPAD4* already at 2h, while *MtVSP1* expression was strongly induced at 4h and 6h following *WF* treatment (**Supplemental Figure 1**).

24h after stimulation *M. truncatula*, we tested the performance of fungal pathogen *Botrytis cinerea* on systemic leaves distal from the stimulated leaves. The *WF* treatment reduced the area of necrotic zones under *Botrytis* inoculation site compared to water controls, characteristic of systemic acquired resistance (SAR) (**Supplemental Figure 2**). Together with marker gene expression data, the *WF* treatment appeared to produce early local leaf responses as well as systemic responses that contribute to altered

pathogen performance in our experimental system. Therefore, this treatment was chosen as a sender plant trigger for evaluating receiver plant responses in the following experiments.

CMN mediates receiver plant responses to stimulation of signal senders

We grew two *Medicago truncatula* seedlings in a single pot, each in a separate 30 µm nylon mesh pocket that allowed AMF hyphae and root exudates to pass through while preventing direct root contact. One of the plants in each pot was inoculated with *Rhizophagus irregularis* spore suspension for seven weeks to establish a CMN between the two plants. In the CMN disconnection treatment (henceforth "cut"), we severed the CMN between plants using a blunt knife. In the CMN "connected" treatment, we preserved CMN connectivity, leaving the space between plants uncut. However, to separate the effects of CMN disruption from mere hyphal damage, we disrupted the extraradical hyphal network at the far edge of the "connected" pot. This approach controlled for potential plant responses to wounded AMF hyphae, allowing us to isolate the effect of CMN continuity - a key aspect missing from previous studies[9,10]. Moreover, the nylon mesh pockets also protected plant roots from accidental wounding during the CMN perturbations. Next, we mechanically wounded and applied *flg22* to the sender leaves or treated with water as the control (**Figure 1A).**

To test whether there is any effect of the position of hyphal network perturbation without induced sender signals, we compared receiver responses to water treated senders in the pots with "cut" and "connected" CMN. Importantly, there was no significant transcriptomic change detected when the "cut" and "connected" treatments were compared (**Supplementary Figure 3**), strongly indicating that, firstly, the hyphal damage was likely applied evenly in both CMN treatments and, secondly, the position of the CMN interference alone does not contribute to any significantly differentially expressed genes (DEGs) in receiver plants. Therefore, this result permits a fair comparison how the integrity of inter-plant CMN connection contributes to unique receiver responses after sender stimulation by mechanical wounding and *flg22* application. To further test this, we stimulated the sender plants and compared receiver responses to non-stimulated senders in the "cut" and "connected" CMN treatments (**Figure 1)**.

We found that naïve receiver plants display distinct transcriptional responses to sender stimulation when CMN is cut compared to uncut inter-plant connection (**Figure 1B**). We identified 1880 up- and 3005 down-regulated DEGs that characterise CMN connection dependent receiver responses (**Figure 1B**). Among them, there were 15 DEGs that even showed opposite regulation in the cut and connected treatments (**Supplemental Table 1; tab-D)**. Twelve DEGs, including *M. truncatula* homolog of plant defence gene *PHATHOGENESIS RELATED 1* (MtrunR108HiC_038642), were significantly downregulated in the receiver plant connected by CMN but upregulated in disconnected CMN. In contrast, transcription factor NAC25 (MtrunR108HiC_019250) and a few receptor kinases such as peptidoglycan-binding LysM domain protein (MtrunR108HiC_035065) and RLK-Pelle-LRR-XII-1 family kinase (MtrunR108HiC_036113) were upregulated in the receivers with connected CMN but downregulated in the cut treatment.

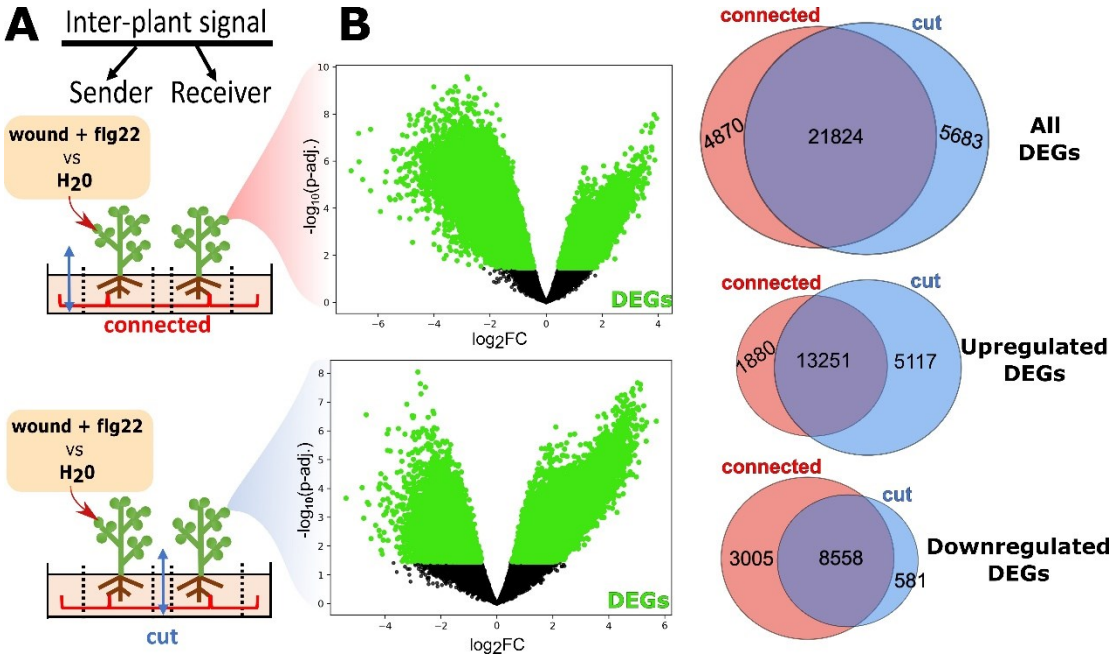

Figure 1. CMN connection contributes to wound and flagellin induced inter-plant responses. (A) A duet of *Medicago* plants were grown in 30 µm mesh pockets (dashed lines) and inoculated with AMF *Rhizophagus iregularis* to form CMN (red). Positions of mycorrhizal hyphal network cut are indicated with a blue double-head arrow. Sender plants with the cut-CMN and the CMN connection were stimulated by wounding and *flg22* application to measure responses in the receiver plant leaves. **(B)** Wounded and *flg22 (WF)* treated plants were firstly compared to corresponding H_2O treatments in each CMN treatment respectively to identify up- and down-regulated responder plant DEGs. After, the DEGs in CMN connected pots (red circles) and the cut-CMN (blue circles) were compared. Volcano plot displays log10 of p-adj. and log_2-fold change for each transcript in the *(WF)* comparison with water controls. Each treatment contained four biological replicates (N=4). Full list of DEGs, their annotations, fold change and FDR values are available in **Supplemental Table 1**.

CMN-dependent inter-plant signals transcriptionally remodulate plant defence

Interestingly, gene functions relating to DNA metabolic processes - DNA repair (integration) and phosphotransferase activity - were significantly enriched within the 1880 upregulated DEGs (**Supplemental Figure 4; Supplemental Table 2 tab-A).** Functions with the most significant enrichment by downregulated DEGs were related to translation, RNA binding and processing, ribosomal subunit structure and organization as well as plant stress responses - primarily ROS metabolism, response to stimuli and jasmonic acid (**Supplemental Figure 5; Supplemental Table 2 tab-B).**

GO-term annotation was available for around 84% of the 4885 DEGs specific to the uninterrupted CMN treatment (**Supplemental Table 2 tab-C),** representing a good functional assessment. Complementary, we also performed an independent *de novo* functional prediction with all *M. truncatula* mRNA fasta sequences using *Mercator* ortholog-based function inference. Congruent with GO-term analysis, the *Mercator* enrichment analysis listed protein phosphorylation and phosphotransferase activity to be enriched by the upregulated DEGs **Supplemental Table 2 tab-D** and

211 RNA processing and protein biosynthesis **Supplemental Table 2 tab-E** by the
212 downregulated DEGs.
213 Intriguingly, after careful inspection of the original bin descriptors from the
214 automated *Mercator* annotation (**Supplemental Table 3 tab-A)**, it was evident that
215 many of the pre-assigned bins also relate to plant defence (**Supplemental Table 3 tab-**
216 **B).** Therefore, we adopted a similar approach to the recent study in *Arabidopsis*[13] and
217 manually assigned a complementary ''Defence signalling & response'' functional bin
218 (**Supplemental Table 3 tab-C)** for more accurate functional classification within the
219 original hierarchy of *de novo* prediction by *Mercator* (**Supplemental Table 3 tab-D).**
220 Interestingly, the curated ''Defence signalling & response'' category contained
221 higher cumulative transcript fold change of the 4885 DEGs for the CMN connected
222 compared to the 5683 DEGs specific to the cut CMN treatment (**Figure 2A**) and
223 displayed the strongest *WF* treatment induced inter-plant responses alongside protein
224 biosynthesis and photosynthesis in receivers with inter-plant CMN connection
225 (**Supplemental Table 3 tab-E**). The defence signalling & response in CMN
226 "connected" receivers showed downregulation of enzymes involved in ROS
227 homeostasis, receptor-like kinases and intracellular MAPK and Ca-dependent kinases,
228 as well as Ub-proteasome pathway (**Figure 2B**). Furthermore, genes involved in
229 jasmonic acid synthesis and perception were downregulated compared to salicylic acid
230 pathway. In addition, receiver plants displayed clear transcriptional changes in genes
231 encoding specialized metabolites such as terpenoid and flavonoid synthesis.
232 An intriguing observation is the relatively high number of upregulated and low
233 number of downregulated DEGs which are represent exclusive responses in the
234 receivers with cut CMN compared to connected CMN (**Figure 1B**). Certain gene
235 functions such as cell division, protein glycosylation, amino acid and nucleotide
236 metabolism appear to be more enriched in the cut treatment (**Figure 2A**). Interestingly,
237 when we investigated plant stress and defence related functions (**Supplemental Figure**
238 **7**), most of the transcripts from the cut CMN treatment displayed upregulation in sharp
239 contrast to downregulation in the connected CMN treatment (**Figure 2B**). This strongly
240 indicates that the receiver responses are highly influenced by the CMN integrity. Given
241 that plant volatiles were not restricted neither in connected or cut treatment, this finding
242 may suggest that the receiver responses to CMN-mediated signals could interact with
243 responses from inter-plant volatile signals to affect gene regulation via yet unknown
244 mechanisms.

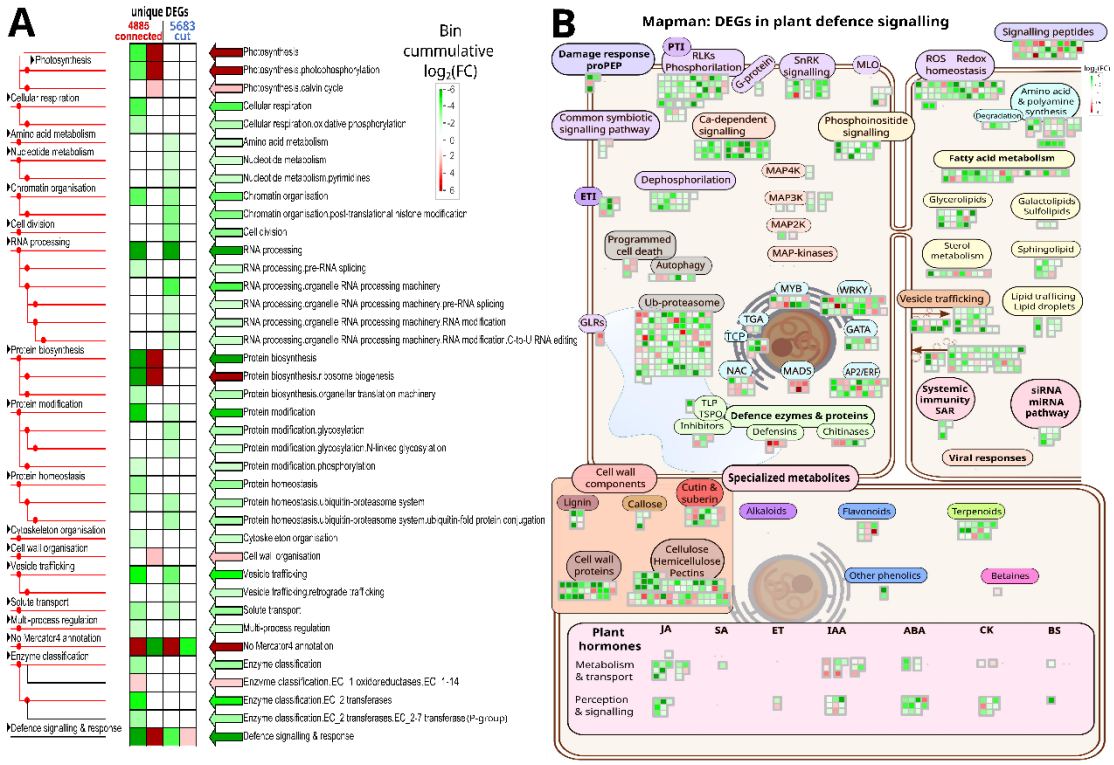

Figure 2. CMN connection is required for remodelling of biotic stress responses in inter-plant signal receivers. (A) Cumulative transcript fold changes of plant functions encoded by up- (red) and down-regulated (green) DEGs display different and specific responses to sender stimuli in the connected and cut CMN treatments. Visualisation is based on *Mercator4* functional annotation via *PageMan.* The ranked enrichment for each category is provided in **Supplemental Table 3 tab-E.** (**B**) 884 DEGs corresponding to plant biotic stress responses and plant defence signalling display dramatic transcriptional responses in responders with inter-plant CMN connection. Green colour represents downregulated, red – upregulated DEGs with colour intensity proportional to their $\log_2$FC. List of displayed DEG annotations and individual fold-changes is provided in **Supplemental Table 1 tab-B.** The image file for *MapMan* visualisation of ''Defence signalling & response'' pathways is available for download as **Supplemental figure 6.** Mapping file containing bin-assignment to immune receptors, intra-cellular signalling components and other defence related functions is available in **Supplemental Table 3 tab-D.**

Inter-plant signals modulate volatile and metabolite composition in CMN-dependent manner

To further test whether inter-plant CMN connection influences the potential infochemical production and composition in receiver plant, leaf metabolites and volatiles were analysed using untargeted metabolomics approach. When *Medicago* senders were wounded and treated with *flg22* (**Figure 3A**), CMN-connected responders display significantly reduced production of volatile leucinamide (V2) and increased production of monoterpenoid β-fenchyl alcohol (V5) alongside several other leaf compounds such as medicagenic acids (L45; L47), acetylsoyasaponin (L46), genistein 7-O-glucoside (L15), 1H-Indole-3-acetaldehyde (L3), tyrosine (L8) and hex-bayogenin (L42) when compared to the H_2O treated senders (**Figure 3B**). Notably, these compounds were not significantly over- or under-produced in inter-plant signal

receivers with the interrupted CMN, suggesting CMN-dependent metabolic changes to neighbour signals. Instead, leaf metabolites soyasapogenol E (L51) and ethyl-D-glucopyranoside (L9) were significantly upregulated while mannopyranoside compound (L52), chrysoeriol (L19) and tricin GlcAGlcA (L20) were downregulated in receivers with the cut CMN (**Figure 3B**). Interestingly, receivers with the interrupted CMN did not show significant change in any measured volatile production unlike receivers with the CMN connection.

All leaf samples for metabolomics were collected from the same plants as the samples for RNA-seq, enabling investigation whether the is correlated change in leaf metabolites and defence gene expression using the set of 4885 DEGs specific to wounding and *flg22* response in CMN connected receivers. Surprisingly, proline (L5) and soyasapogenol E (L51) demonstrated the strongest correlation with a number of genes involved in plant defence responses (**Figure 3D),** including plant surface LRR Ser/Thr kinase receptors, including the flagellin receptor *FLS2*, *PATHOGENESIS RELATED 4,* E3 Ub ligases PUB22 and PUB23, ethylene and gibberellin response factors as well as several transcription factor families, especially MYB-related and GRAS. Additionally, aquaporin gene *NIP2* expression was strongly correlated with production of ethyl-D-gluccopiranoside (L9) and HO-α-muurolene (V24) (**Figure 3D**).

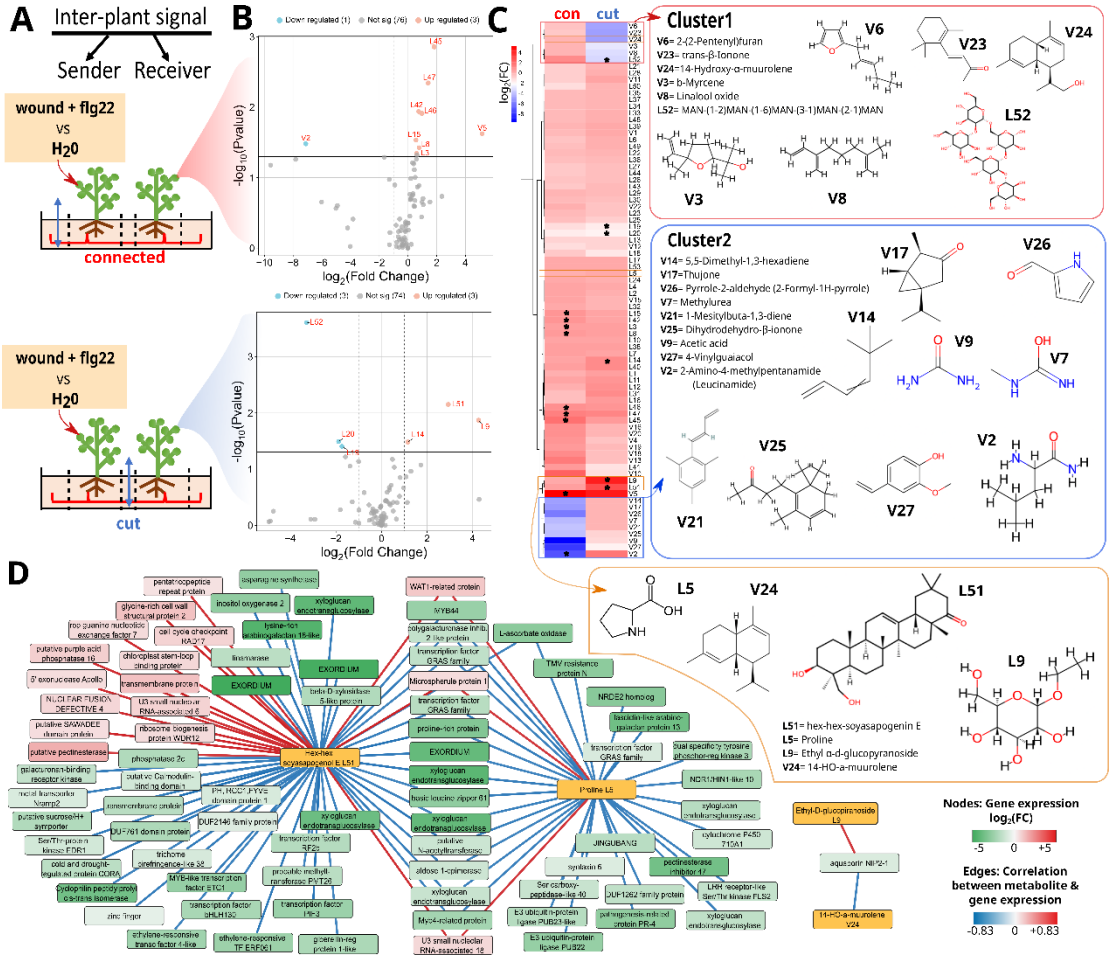

Figure 3. CMN modulates leaf metabolite and volatile production in response to neighbour stress-induced signals. (A) Two *Medicago* plants were grown in 30 µm mesh pockets (dashed lines) and inoculated with AMF *Rhizophagus iregularis* to form CMN (red).

297 The blue double-head arrow indicates the position of CMN interruption prior to sender plant
298 wounding and *flg22* application to measure responses in the receiver plant leaves. **(B)** Volcano
299 plots displaying down-regulated or up-regulated leaf metabolites (L) and volatile compounds
300 (V) when comparing inter-plant responses to wound and *flg22* with H_2O controls in receivers
301 with connected (top) or cut (bottom) CMN. **(C)** Hierarchical clustering of colour-coded $\log_2$
302 fold changes (FC) for all 53 detected leaf metabolites and 27 volatiles. Two clusters of
303 compounds display the largest relative differences in receiver responses to inter-plant stress
304 signals between connected (con) and cut CMN treatments. The asterisks indicate significant FC
305 based on the volcano plots in panel **B**. Chemical structures are based on ChemSpider and
306 PubChem databases for the closest matching compounds. **(D)** The network produced by
307 regularized canonical correspondence (rCCA) analysis displays the correlation between
308 normalized CPMS read counts of 4885 DEGs (identified in **Fig. 1**) with relative metabolite
309 quantities. Only correlations with threshold >0.7 are displayed and include 4 metabolites
310 (orange). The available homology-based gene function predictions from MtrunR108_HiC
311 reference genome are mapped on the network along with colourcoded gene expression changes
312 in CMN connected receivers. The source data for metabolite identification and network
313 generation are provided in the **Supplemental Table 4.** Analytical standards were used to
314 quantify selected metabolites and validate correspondence to independent samples in
315 **Supplemental Figure 11**.

316

317 *CMN mediated inter-plant signals induce acquired susceptibility to Botrytis cinerea*
318 *but resistance to Fusarium sporotrichoides*

319 Since we identified CMN-dependent changes in receiver plant biotic stress
320 genes and leaf metabolites with reported functions in plant-pathogen interactions, we
321 wished to test whether stressed sender plants modulate resistance to known plant
322 pathogens in CMN connected receivers. We evaluated leaf infections by two plant
323 generalist fungal pathogens - *Botrytis cinerea* and *Fusarium sporotrichoides*.
324 Importantly, when the inter-plant CMN connection was cut, there was no significant
325 difference in receiver lesion size upon *B. cinerea* or *F. sporotrichoides* infection
326 between sender treatment of WF and water (**Figure 4B**). Interestingly, when we added
327 generalist pathogen *F. sporotrichoides* to naïve receiver plants, the necrotic lesions
328 were significantly smaller when sender plants were wounded and treated with flagellin
329 (neighbour-primed) compared to water treated senders (**Figure 4A**), suggesting inter-
330 plant signal induced resistance to the pathogen attack. However, when we exposed
331 CMN connected naïve receiver plants to another pathogen *B. cinerea*, the necrotic
332 lesions were significantly larger when sender plants were wounded and treated with
333 flagellin compared to water treated senders (**Figure 4A**). Surprisingly, this effect was
334 the opposite to intra-plant signals induced by wounding and flagellin treatment of distal
335 leaves (SAR) which originally reduced lesion size in *B. cinerea* infected distal leaves
336 (**Supplemental Figure 2**). This suggests that intra- and inter-plant signalling induced
337 by wounding and flagellin may lead to different outcomes, possibly due to distinct
338 underlying mechanisms. Our findings underscore the important role of the intra-plant
339 CMN connection in how stress-induced signals affect pathogen resistance in
340 neighbouring plants. Additionally, we highlight that stress-induced inter-plant signals
341 in mycorrhiza-connected plants can result in varying levels of tolerance to different
342 fungal pathogens in the receivers.

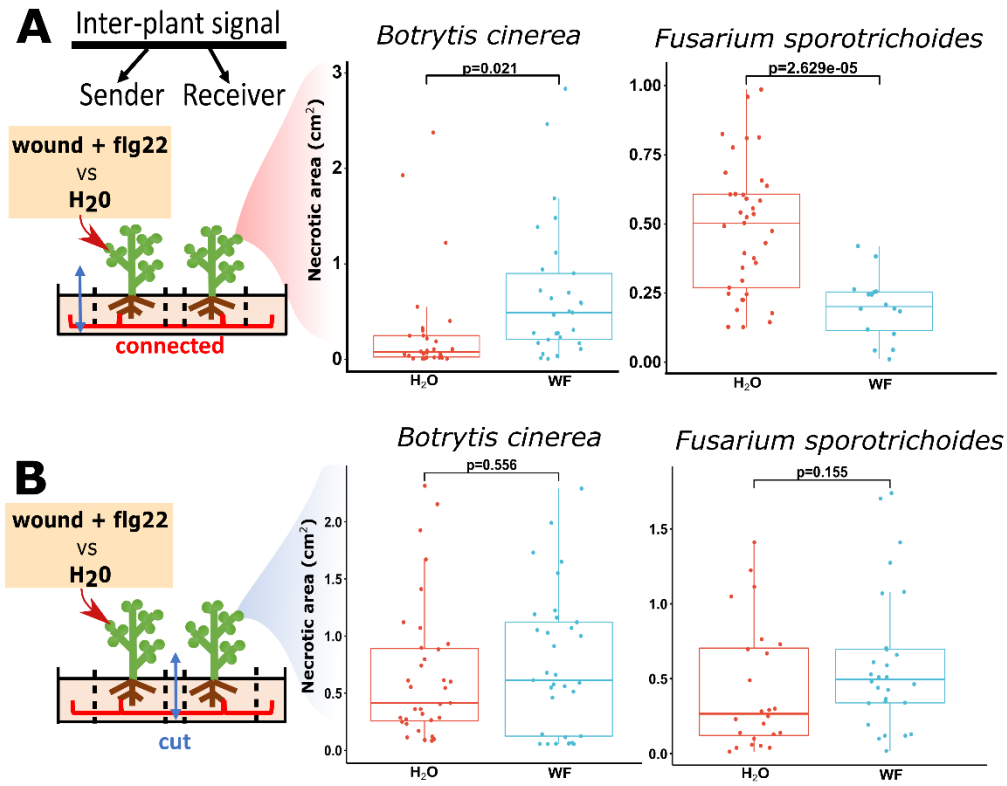

Figure 4. Stress-induced inter-plant signals modulate resistance to fungal pathogens in CMN connected plants. A. Size of necrotic lesions on *Mediago truncatula* leaves 72h after inoculation with *Botrytis cinerea* and *Fusarium sporotichoides* in CMN-connected plants. Wounding and flagellin (WF) treatment of sender plants induces resistance to *F. sporotrichoides* (F=21.355; p=2.629e-05) but susceptibility to *B. cinerea* (F=5.6603; p=0.02066). **B.** Size of necrotic lesions on *Mediago truncatula* leaves 72h after inoculation with *Botrytis cinerea* and *Fusarium sporotichoides* in receivers with cut CMN. WF treatment of sender plants does not significantly alter receiver plant lesion size upon *F. sporotrichoides* (F=2.089; p=0.1545) or *B. cinerea* (F=0.3496; p=0.5563) infection compared to receivers next to the H_2O treated senders. Experiments in panel A and B were performed independent from each other. Pathogen assays in each graph were repeated independently 3-times and represented as pooled data. Line indicates the median, boxes represent the interquartile range (IQR), whiskers - variance within 1.5xIQR. Detailed comparison of all 3 individual experiments for each panel along with normality tests and repeated measures analysis is provided in **Supplemental figure 8**. Each treatment contained ≥8 biological replicates (receiver plants) per experiment.

Discussion

CMN as a mediator for inter-plant information exchange

For a few decades, CMN has been hypothesised to function as an inter-plant signalling conduit[3,4,14]. However, to date our mechanistic understanding on the molecular responses to stress induced signals in mycorrhizae-interconnected plants has been limited by very few empirical studies. Importantly, the interruption of CMN in

367 tomato[9] or pea[10] plants was confounded by physical damage to symbiotic hyphae.
368 Moreover, the few existing studies were all based on the targeted gene expression or
369 enzyme activity measurements[9,15], rather than characterising global responses of
370 receiver plants to reveal the key pathways involved in the CMN-mediated neighbour
371 priming against pathogens in an unbiased way. In this study, our experimental design
372 allowed us to separate the effects of CMN disconnection from damage to the symbiotic
373 hyphal network (**Supplemental Figure 3**). While *in vitro* studies have reported the
374 capacity for reestablishment of hyphal connections after hyphal cutting[16], the rate of
375 hyphal growth, estimated to be around 10-20µm/h in vitro[17] or 1-3mm/d on soil[18] would
376 not exceed the distance between nylon mesh in our experiment and unlikely to confound
377 the experimental results.
378 For the first time, using an untargeted approach, we have identified a unique
379 profile of volatiles, leaf metabolites, and transcriptional responses in receiver plants
380 that share an AMF connection with biotic stress-stimulated signal senders, compared
381 to plants with severed AMF connections (**Fig. 1, Fig. 3**). Furthermore, this manifested
382 in altered plant susceptibility to pathogenic fungi *Botrytis cinerea* and *Fusarium*
383 *sporotrichoides* **(Fig.4**). Together our study implicates CMN as important players for
384 defence signal exchange. To establish this as a general phenomenon within plant
385 communities in nature and agricultural systems, future research should expand the
386 experimental scope to include diverse AMF and plant taxa and investigate the
387 communality of plant regulatory and metabolic pathways that are modulated by
388 neighbour signals. Furthermore, extended effects of CMN-mediated inter-plant signals
389 to nodulation and plant interaction with plant growth promoting bacteria is another
390 important avenue for future research in legume and non-legume crops and ultimate
391 harnessing of CMN functions for agriculture.
392
393 *CMN contribution to modulation of inter-plant defence and metabolic responses*
394 The majority of receiver leaf compounds responding to CMN-mediated
395 neighbour signals are implicated in plant defence during biotic stress. One of the
396 important key metabolic changes highlighted was the increased production of
397 triterpenoid saponins (including hex-bayogenin (L42), medicagenic acids and their
398 derivatives L45-L47) (**Fig. 3B**). Interestingly, medicagenic acids, bayogenin and other
399 saponins are well-known important legume triterpenoids that act as phytoanticipins
400 (preformed defence compounds) and phytoalexins (induced defence compounds),
401 contributing to defences against pathogens by perturbing microbial membrane integrity
402 [19–23]. Additionally, levels of numerous monoterpene leaf volatiles were among the most
403 notable differences between receivers in the connected and cut treatments (**Fig. 3C**).
404 Monoterpenoid α-muurolene along with other terpenoids from endophytes of
405 *Catharanthus roseus* are known to display antifungal properties[24]. These compounds
406 display interplant stress-induced production in CMN connected receivers but not in the
407 cut receivers.
408 Interestingly, receiver plants with intact AMF connection displayed increased
409 production of 1H-Indole-3-acetaldehyde (IAAld) (L3) – an intermediate for auxin
410 synthesis. As reviewed[25] auxins have important roles in plant-microbe interactions.
411 Curiously, *P. syringae* strain DC3000 produces IAA as a plant virulence factor from
412 IAAld using dehydrogenase AldA in order to supress salicylic acid-mediated defenses

413 in *A. thaliana*[26]. Furthermore, many auxin efflux proteins were significantly
414 upregulated in the connected CMN treatment (**Supplemental Table 5 tab-A**). Among
415 them was vacuolar auxin transporter *WALLS ARE THIN1 (WAT1)*-related gene
416 *MtrunR108HiC_014019. AtWAT1* is also known to be involved in cell wall thickening
417 [27]. Since CMN connected plants also displayed transcriptional changes in cell wall
418 components as well as auxin synthesis and perception **(Fig. 2)**, we hypothesise that
419 auxin homeostasis may in part contribute to cell wall remodelling and specialized
420 metabolite production in defence against pathogens in CMN connected *Medicago*
421 plants.
422 The integrity of CMN was not only responsible for increased metabolite
423 production but also suppressed specific metabolites in response to neighbour signals.
424 Certain triterpenes such as ethyl-D-gluccopiranoside (L9) or soyasapogenol E (L51)
425 demonstrated more pronounced induction in the cut CMN treatment as opposed to the
426 connected treatment, suggesting that CMN mediated inter-plant signals may dampen
427 the inter-plant effects of other CMN independent signals. Soyasapogenol E levels were
428 negatively correlated with expression of several ethylene response factors and members
429 of MYB and GRAS transcription factor families (**Figure 3D)** which were well
430 represented among the 4885 DEGs specific to the connected treatment (**Supplemental**
431 **Table 6 tab-A)** and may indicate their regulatory roles in triterpenoid production.
432 CYP450s and UDP-glycosyltransferases (UGTs) are primarily involved in mevalonate-
433 dependent isoprenoid biosynthesis, including monoterpenes, sesquiterpenes and
434 triterpenes[28]. We found sets of up- and down-regulated CYP450 and UGT enzyme
435 transcripts that are specific to the cut and connected treatments (**Supplemental Table**
436 **6 tab-B)** and could be involved in the observed CMN-dependent differences in
437 metabolite production. Lastly, leaf proline content was significantly correlated with
438 expression patterns of several genes involved in plant defences, including *flg22* receptor
439 *FLS2* and several E3 Ub ligases (**Figure 3D)**. Proline and its derivatives pyrroline-5-
440 carboxylate are involved in plant responses to abiotic and biotic stress, including
441 pathogens defence and mitigation of oxidative damage by scavenging reactive oxygen
442 species (ROS)[29,30]. While the relative changes in proline content after sender
443 stimulation were not significantly different between the cut and connected treatments
444 (**Figure 3C)**, genes involved in ROS production and scavenging were significantly
445 enriched among the 4885 DEGs specific to the connected treatment **(Supplemental**
446 **figure 5)**.
447
448 *Ecological and evolutionary roles of CMN-mediated inter-plant signals*
449 CMN transmitted inter-plant stress signals have been previously considered to
450 provide fitness benefits the receiver by providing increased pathogen resistance [9] and
451 recruitment of natural enemies[10]. However, our data on differential inter-plant *M.*
452 *truncatula* responses to *B. cinerea* and *F. sporotrichoides* infection clearly
453 demonstrated that the outcome may not always be positive for the receiver. We
454 emphasise that the potential beneficial effects from eavesdropping on conspecific
455 signals via CMN must be holistically studied in context of different pest and pathogen
456 species as well as host genotypes. Intriguingly, neighbour-modulated susceptibility
457 (NMS) has been documented in rice and durum wheat growing next to pathogen free
458 conspecifics of different genotypes and appears to be mediated by inter-plant signals in

459 soil [31]. In particular, the study showed that wheat growing next to a different conspecific
460 genotype display increased susceptibility to hemibiotroph *Zymenoseptoria tritici* but
461 reduced susceptibility to biotroph *Puccinia triticina,* suggesting different production or
462 perception of signals by different plant genotypes. Similarly, *Magnoporthe oryzae*
463 showed fewer lesions on rice neighbouring a different conspecific genotype compared
464 to isogenic cultivar, while another hemibiotroph *Bipolaris oryzae* demonstrated more
465 lesions [31]. *Arabidopsis* plants exposed to elicitors in insect eggs are able to produce
466 inter-plant signals that induce broad spectrum resistance against bacterial pathogen
467 *Pseudomonas syringae* [1] and fungus *Botrytis cinerea* [32], suggesting that certain plant-
468 to-plant signals may be potentially more conserved and less specific to different
469 pathogen species. This further highlights the need to test a range of different elicitors
470 on senders and evaluate responses in responders of different genotypes and species in
471 the future experiments.
472 However, in our foundational experiments presented herein we wished to use
473 stimuli or elicitors that would give consistent and reproducible PAMP or DAMP
474 responses without the added complexity and potential variability of using live herbivore
475 or pathogen infections. For example, insect oral secretions are known to contain
476 additional chemical elicitors that are recognised by plant HAMP receptors or deliver
477 insect effector proteins that supress plant defence responses[33]. Similarity, microbial
478 pathogens produce effectors that either supress PTI responses in plants or induce
479 effector-triggered immunity (ETI)[34], thus introducing mechanistic complexity for the
480 generation of systemic and inter-plant signals in the senders. Furthermore, different
481 feeding guilds of herbivores, such as cell-content feeding, leaf or root chewing, stem or
482 leaf boring, phloem or xylem sucking, as well as the range of pathogens with biotrophic
483 to necrotrophic lifestyles and diverse effector repertoires offer an extended scope for
484 future investigations on plant-to-plant responses to these diverse interactions.
485 Neighbour induced susceptibility or resistance would provide opposing selective
486 pressures for the evolution of specific signal generation and perception mechanisms
487 along with receiver responses. For example, volatiles are known for their roles in
488 pollinator as well as parasitoid attraction. Since *Medicago truncatula* is primarily a self-
489 pollinator, it is unlikely that the altered receiver VOC profiles would affect plant
490 reproductive fitness directly but may be important in other outcrossing species.
491 Interestingly, volatile monoterpenes (e.g., penene, campene, sabinene) have been
492 shown to induce inter-plant systemic acquired resistance (SAR) against *Pseudomonas*[2]
493 and could potentially relay SAR signals from plant-to-plant[35]. While we did not find
494 changes in the same monoterpene compounds[2] it would be intriguing to test whether
495 VOCs could further propagate and amplify CMN-mediated inter-plant signals and thus
496 affect plant defences at a community level. Moreover, VOC and specialized metabolite
497 composition is very diverse across angiosperms. For example, the lineage-specific
498 number and expansions of terpene synthase genes across angiosperms suggest
499 functional divergence in terpene structure and regulation in different ecological
500 conditions and plant genotyopes[36–38]. Therefore, metabolic effects of CMN-mediated
501 inter-plant stress signals could have diverse effects in crops under field conditions.
502
503
504

Conclusion

Receiver plants' biotic stress responses and defence signalling pathways can be uniquely shaped by inter-plant signals transmitted via CMN and manifest in differential disease outcomes. These findings underscore the potential pivotal role of CMN in modulating plant immunity at a community scale, revealing a sophisticated and nuanced mechanism of pathogen-specific susceptibility and resistance. This insight prompts further investigation into the mechanisms of CMN-mediated interplant signalling, which could be transformative for understanding plant defence dynamics in complex natural ecosystems and for optimizing disease management strategies in agriculture.

Materials and Methods

Plant growth

30 µm pore size autoclavable PA6-grade nylon mesh (JPP140 from Technical textiles, Ekobalta, Latvia) was used to make 11 cm wide and 10 cm deep pockets which were filled with autoclaved soil:sand mixture (3:1 v/v). Soil (gardening substrate with black earth) was purchased from Biolan Baltic OÜ (pH: 6,0; EC: 25 mS/m; N~100 mg/L; P~60 mg/L; K~200 mg/L; peat fraction<20mm). Quartz sand (grain size ≤0.5mm) obtained from SACRET®, Latvia. Two substrate filled mesh pockets were placed into 1L black plastic pot (11x11x12 cm L x W x H) and surrounded with the surplus soil:sand mixture to prevent them from touching each other or the edge of the pot. *Medicago truncatula* R108 seeds were scarified with a sterile scalpel and germinated on wet *Whatman* filter paper for 2-3 days before planting onto the soil:sand mixture within each mesh pocket. The images of the setup are provided in the **Supplemental Figure 9**. Plants were grown in growth cabinet (SANYO MLR-351H, Japan) at 20°C, 50%RH, 16h day / 8h night cycle using a set of twelve 6500K (3200lm) and three 2700K (3350lm) fluorescent lightbulbs (T8 MASTER TLD G13 Philips, 36W) to cover the entire PAR spectrum with 300 mmol m^2 s^{-1} light intensity. Each pot was watered with 200mL 0.5X Hoagland nutrient solution once a week.

AMF cultivation & inoculation

Rhizophagus irregularis (DAOM 197198) was cultivated on *Daucus carota* hairy root cultures [39–41], grown on M-media (1% sucrose, 0.4% Gelrite gellan gum) at 25°C in darkness. 6-month-old cultures were processed for *R. irregularis* spore collection using 10mM citrate buffer (pH=6) to dissolve spore-containing solid media and capture spores within 40µm cell stainer (SPL Lifesciences) and resuspend in sterile dH_2O. Spore density was determined microscopically. Suspension volume containing 200 spores was applied to one of the seedlings in the pot. Plants were grown for 7 weeks to establish CMN between the sender and receiver plants. The colonization status of the receiver plant was verified using ink-vinegar staining method [42] after the experiment.

Treatment of CMN and sender plants

7-weeks post AMF inoculation all experimental pots were divided into two groups: 1) uninterrupted CMN (sender-receiver plants remain connected via CMN) where a blunt knife was inserted into the soil along the edge of the pot as a control and

551 2) a group of cut CMN where a blunt knife was inserted into the soil between the mesh
552 pockets to disrupt the CMN connection between signal sender and receiver plants as
553 depicted in **Supplemental Figure 9**. Three days after this manipulation, sender
554 *Medicago* plants were subjected to mechanical wounding by applying three squeezes
555 with metal forceps to each leaflet of two fully expanded trifoliate compound leaves,
556 followed by the application of a 5 µL drop of synthetic 1 µM bacterial flagellin (*flg22*,
557 MedChemExpress, Sweden) on each forceps-wounded leaflet. 5 µL of dH_2O without
558 mechanical wounding was used as the control treatment. Receiver plants were left
559 untreated and collected 3 days after the stimulation of the sender plants.
560
561 *RNA extraction & transcriptome sequencing*
562 Three separate trifoliate leaves from 8-weeks old receiver plants were harvested
563 in liquid N_2, homogenized with pestle and mortar for RNA extraction using
564 ReliaPrep™ RNA Miniprep System (Promega, cat. Z6012). RNA quantification was
565 performed with Qubit™ RNA BR Assay Kit and Agilent Bioanalyzer RNA 6000 Pico
566 Kit. Samples from 4 different plants were processed as biological replicates for each
567 treatment. Total 400ng of each RNA sample (RIN≥7, $OD_{260/280}$ between 1.9-2.1,
568 $OD_{260/230}$ between 1.5-2.0) was processed for library preparation using MGIEasy RNA
569 Directional Library Prep Set following manufacturer's instructions. QIAseq
570 FastSelect –rRNA Plant Kit (QIAGEN) was used to deplete rRNA prior to the library
571 fragmentation step. Qubit® dsDNA HS Assay and Agilent HS DNA Kit was used to
572 determine library concentration and length (average 326 nt) prior to multiplexing and
573 circularization. The final pooled libraries (1.94 ng/µL) were sequenced on DNB
574 G400RS high throughput sequencing machine (MGI) using FLC PE150 flowcell.
575
576 *Raw data processing and DEG analysis*
577 Read filtering and adapter removal was performed with *fastp 0.20.0* (default
578 parameters; read trimming >100 bp). *STAR 2.7.10a* [43] was used to map the reads against
579 *Medicago truncatula R108* reference genome available in
580 https://medicago.toulouse.inrae.fr/MtrunR108_HiC (INRA, Toulouse). *SortMeRNA*
581 *version 4.3.6* [44] was used to quantify and filter rRNS using smr_v4.3_default_db
582 database. DEG analysis was performed with *limma* (Bioconductor)[45]. Low count
583 features were filtered using the function *filterByExpr* implemented in *edgeR* (v4.6.2).
584 *Voom* with quality weights was used to transform the data prior to linear modelling with
585 *limma*. Features with FDR < 0.05 were regarded as statistically significant and used for
586 downstream selection of CMN connection specific interplant responses.
587
588 *Functional enrichment analysis*
589 Enrichment of GO biological and molecular functions for DEGs was calculated
590 using *agriGO v2.0* [46] Fisher exact test (FDR) with *MtrunR108_HiC_functional*
591 *annotation* file as reference and visualized with enrichment bubble *SRplots*. To
592 independently validate our enrichment analysis, we performed complementary
593 enrichment analysis with the *de novo* gene function predictions obtained with
594 *Mercator4 v2.0* tool[47]. To this end, *MtrunR108_HiC.1.0.fasta_features* (all genomic
595 mRNA nt sequences) were used as input for the gene orthology search (**Suppl. Table**
596 **3; tab-A**). The automated function descriptors were manually checked and

complementary assigned to "Defence signalling and response" bin (**Suppl. Table 3; tab-B**). Since a distinct and comprehensive ''plant stress and defence'' function category was originally absent from the automated functional assignment (**Suppl. Table 3; tab-A**), we extracted the corresponding gene identifiers, and *de novo* compiled the 'plant stress and defence'' bin (BINCODE 80) (**Suppl. Table 3; tab-C**). This list was then combined with the original list of Mercator4 functions from **tab-A** to produce an updated input (mapping) file for functional enrichment analysis, available in **Suppl. Table 3; tab-D**. Subsequent visualisation of DEG functions was performed with *MapMan v3.7* [48] and *PageMan* [49] functional annotation tools. Statistical analysis on DEG enrichment for *MapMan* pathways was performed using built-in Wilcoxon rank test and Benjamini-Hochberg (BH) p-value correction[50]. The graphical overview of plant defence pathways displayed in **Fig. 2** was drawn manually in *Inkscape* and loaded as separate pathway image file into *MapMan* (available for public download as .jpeg in **Figure supplement 6** and reusable by citing this manuscript).

rt-qPCR

To verify the expression data from RNA-seq dataset, we performed rt-qPCR on selected genes from independent samples. Test genes were selected based on the largest FC difference among connected and cut treatments (**Supplemental Figure 10A**). Reference gene candidates were selected based on the lowest fold change across all treatments (**Supplemental Figure 10B**). *M. truncatula* gene specific primers were designed in NCBI Primer BLAST for 100-200 nt amplicons spanning exon-intron junction where possible. cDNA was synthesised with *Maxima First Strand cDNA Synthesis Kit (Thermo Fisher Scientific)* and qPCR performed with *Maxima SYBR Green/ROX qPCR Master Mix (2X) (Thermo Fisher Scientific)* on *ViiA™ 7 Real-Time PCR System (Applied Biosystems)* and analyzed with the native *QuantStudio 7 Pro 1.6.1* software. Primer efficiency (E%) was calculated using the formula $\left(10^{\frac{-1}{\text{slope}}} - 1\right) \text{x } 100$, with slope being obtained by plotting the $\log_{10}$ values of 10-fold serial dilutions from 1ng to 1ag of purified cDNA (**Supplemental Figure 10E**). The expression of each test gene was normalized by the geometric mean of two selected reference genes (*MtEXO70* and *MtBP28*) using the formula relative expression $= \frac{\sqrt{E_{ref1}^{Ct(ref1)} x\, E_{ref2}^{Ct(ref2)}}}{E_{test}^{Ct(test)}}$, where E_{ref} – primer efficiency of reference gene, E_{test} – primer efficiency of test gene, *Ct(ref)* – Ct value of reference genes, *Ct(test)* – Ct value of the test gene.

Leaf metabolic analysis with LC-HRMS

Metabolome was analysed from the same leaf samples as plant transcriptome by aliquoting 200mg of the frozen homogenized leaf tissues and resuspending in 1.5 mL of 70% methanol, vortexed for 1 minute and left for maceration for 5 days at 4°C in darkness. The obtained extract was filtered through a 0.45 µm filter and injected into the Agilent 1290 Infinity II series HPLC system combined with Agilent 6530 qTOF MS system (Agilent Technologies, Deutschland GmbH, Waldbronn, Germany). Zorbax Eclipse Plus C18 Rapid Resolution HD (2.1×150mm, 1.8µm particle size) column was used at a flow rate of 0.3 mL/min. The column oven was set at 45°C, and the sample injection volume was 3 µL with 40 sec needle wash (70% methanol). The mobile phase consisted of a combination of A (0.1% formic acid in water) and B (0.1% formic acid

642 in acetonitrile). Gradient elution program was used as follows: Initial 5%B, 0-6 min
643 20%B, 6-20 min 40%B, 20-23 min 80%B, 23-28 min 95%B, 28-33 min 95%B, 33-39
644 min 5%B. UV/VIS spectra were recorded at 280 nm and 330 nm. The adjusted
645 operating parameters of the mass spectrometer were set as follows: Fragmentation: 70
646 V; Gas temp: 325°C; Drying gas 10 L/min; Nebulizer 20 psi; Sheath gas temp 400°C;
647 Sheath gas flow 12 L/min. Electrospray ionization (ESI) was used as a source in
648 operating in positive mode. The internal reference masses of 121.050873 m/z and
649 922.009798 m/z (G1969-85001 ES-TOF Reference Mass Solution Kit, Agilent
650 Technologies & Supelco) were used for all analyses of the samples. The Agilent
651 MassHunter Qualitative analysis 10.0 data acquisition software was applied to analyze
652 LCMS data and compare ion fragmentation data with information available in literature
653 and databases, such as METLIN, LIPID MAPS®, Phenol – Explorer, Lotus - Natural
654 575 Products Online and FooDB v1.0 with acceptance mass error ≤ 20 ppm and
655 consistency of isotope/adduct patterns.
656 Analytical standards (L-proline, jasmonoyl-isoleucine, medicagenic acid,
657 apigenin, soyasapogenol B) were used for absolute quantification of matching
658 compounds and their derivatives. External calibration was confirmed at MSI Level 1
659 by co-injection RT match (ΔRT ≤ 3%) and HR m/z for the dominant ESI(+) adduct (±
660 5 ppm). Quantification used external solvent-based calibration (7 levels; 3 replicates
661 per level; linear fit with 1/x weighting when required). No internal standards or matrix-
662 matched/standard-addition approaches were applied. Primary stock solutions were
663 prepared at approx. concentration 0.1 mg mL^{-1} in methanol except jasmonoyl-
664 isoleucine in ethanol, then serially diluted in methanol to the working calibration levels.
665 Validation data are summarised in **Supplementary Table 4 tab-B**. Measured
666 concentrations (µg/g FW) with independent samples are reported in **Supplementary**
667 **Table 4 tab-C.** The correspondence of the repeated experiment and the experiment
668 reported in Figure 3 is displayed in **Supplemental Figure 11**.
669
670 *Plant volatile analysis*
671 Volatile compound analysis was performed using the same leaf samples as the
672 plant transcriptome analysis. The samples were ground into a fine powder using liquid
673 nitrogen, and 100 mg of the homogenized leaf tissue was aliquoted into clean 20 mL
674 headspace vials. A saturated NaCl solution was added to prevent enzyme reactions, and
675 the vials were sealed with Agilent headspace silica gel caps. Each vial was then heated
676 for 20 minutes at 60 °C with an agitator cycle of 30 seconds on and 15 seconds off.
677 Samples were injected into an Agilent Technologies 7820A gas chromatograph coupled
678 with an Agilent 5977B mass selective detector (MSD) using a Gerstel MPS
679 Autosampler. The syringe temperature was set to 130 °C, and the injection volume was
680 2500 µL. A polar CP-Wax 52CB capillary column (50 m × 0.32 mm, 0.20 µm film
681 thickness) with polyethylene glycol was used. Helium (He) served as the carrier gas
682 with a split ratio of 1:20 and a flow rate of 1.2 mL/min. The temperature program started
683 at 60 °C, increased at a rate of 10 °C/min to 250 °C, and was held for 3 minutes. The
684 injector temperature was set at 260 °C. Mass spectra were recorded at 70 eV within an
685 m/z range of 50–500. The ion source temperature was maintained at 230 °C. Compound
686 identification was based on retention indices (determined using a homologous series of

C5–C24 n-alkanes) and mass spectral comparison with the NIST (National Institute of Standards and Technology) MS Search 2.2 library. Data acquisition and analysis were performed using Agilent MassHunter Qualitative Analysis 10.0 software.

Target volatiles (β-myrcene, linalool, β-fenchyl alcohol) were confirmed at MSI Level 1 by retention index (vs C5-C24 n-alkanes) and EI spectral matches to authentic standards. Primary stocks (1 mg mL^{-1} in methanol) were used to prepare calibration standards: each 20 mL HS vial contained 4.7 mL of 30% (w/v) NaCl and 0.3 mL of the appropriate standard solution; working levels were obtained by serial dilution to five concentrations (100–3000 ng mL^{-1}) with three replicate vials per level. Quantification used external calibration (linear regression; 1/x weighting when required). Validation outputs are reported in **Supplementary Table 4 tab-E**.

Correlation of gene expression and metabolite data

Regularized canonical correspondence analysis (rCCA) was used with the *mixOmics* R package (available from Bioconductor; http://www.mixOmics.org) in R studio. R script provided in **Supplementary Table 4 tab-D.** Correlations >0.7 were visualised via *Cytoscape* v3.10.3.

Plant pathogen assays

Fusarium sporotrichoides (Fs) and *Botrytis cinerea (Bc)* were grown on 0.5X PDA at 20°C in darkness for 4 weeks. Mycelial plugs, obtained with a 7.5mm diam. cork borer, were placed on three different trifoliate leaves. Each leaf was placed in a 5.5cm diam. Petri dish with water-saturated filter paper to maintain moisture level. The edge of the petri dish had a pre-cut slit for the leaf petiole to remain attached to the plant throughout the experiment. Plants were placed in shaded at 20°C for 72h. Agar plugs were removed before leaf photography. *ImageJ (Fiji)* was used to measure the area of necrotic lesions.

Data availability

RNA-seq raw data (fastq) are uploaded to NCBI under BioProject: **PRJNA1186668**.

Author contributions (Contributor Role Taxonomy CRediT):

ZO: conceptualization and experimental design (1), data curation (2), formal analysis (3), funding acquisition (4), investigation (5), methodology (6), project administration (7), reagent acquisition and lab resource planning (8), student supervision (10), data validation (11), statistical analysis and visualisation (12), writing (13), reviewing and editing the original manuscript (14)

IN: investigation – metabolic analysis (5), reviewing the original manuscript (14)

EV: formal analysis (3) of pathogen data, investigation – plant-pathogen assays (5), reviewing the original manuscript (14)

DP: investigation – experiment setup, RNA extractions, rt-qPCR (5), reviewing the original manuscript (14)

AK: investigation – experiment setup, RNA extractions, rt-qPCR (5), reviewing the original manuscript (14)

DS: investigation – qPCR validation (5)

AA: investigation – root staining for AMF colonization (5)

KTB: investigation – experiment setup, RNA extractions (5), reviewing the original manuscript (14)
IS: data curation (2), formal analysis (3) of RNA-seq data, reviewing the original manuscript (14)
SJL: conceptualization and experimental design (1), methodology (6), reviewing and editing the original manuscript (14)

Funding

This work was supported by Latvian Council of Science Fundamental and Applied Research grant lzp-2021/1-0056 awarded to ZO and University of Latvia Fundation (*SIA MikroTik* donation).

Acknowledgements

We are grateful to Prof. Yves Poirier group (DBMV, University of Lausanne) for the generous donation of *Medicago truncatula* R108 seeds. We also thank BMC Genome Centre and Bioinformatics Unit support staff for assistance during sequencing and raw data handling.

Competing interest

The authors declare no competing interests.

Literature Cited

1. Orlovskis, Z. & Reymond, P. Pieris brassicae eggs trigger interplant systemic acquired resistance against a foliar pathogen in Arabidopsis. *New Phytol.* **228**, 1652–1661 (2020).
2. Riedlmeier, M. *et al.* Monoterpenes Support Systemic Acquired Resistance within and between Plants. *Plant Cell* **29**, 1440–1459 (2017).
3. Bais, H. P., Park, S.-W., Weir, T. L., Callaway, R. M. & Vivanco, J. M. How plants communicate using the underground information superhighway. *Trends Plant Sci.* **9**, 26–32 (2004).
4. Barto, E. K., Weidenhamer, J. D., Cipollini, D. & Rillig, M. C. Fungal superhighways: do common mycorrhizal networks enhance below ground communication? *Trends Plant Sci.* **17**, 633–637 (2012).

766 5. Brundrett, M. C. & Tedersoo, L. Evolutionary history of mycorrhizal symbioses and
767 global host plant diversity. *New Phytol.* **220**, 1108–1115 (2018).
768 6. Read, D. J. *et al.* Photosynthate transfer from an autotrophic orchid to conspecific
769 heterotrophic protocorms through a common mycorrhizal network. *New Phytol.*
770 **243**, 398–406 (2024).
771 7. Francis, R. & Read, D. J. Direct transfer of carbon between plants connected by
772 vesicular–arbuscular mycorrhizal mycelium. *Nature* **307**, 53–56 (1984).
773 8. Simard, S. W. *et al.* Net transfer of carbon between ectomycorrhizal tree species in
774 the field. *Nature* **388**, 579–582 (1997).
775 9. Song, Y. Y. *et al.* Interplant communication of tomato plants through underground
776 common mycorrhizal networks. *PloS One* **5**, e13324 (2010).
777 10. Babikova, Z. *et al.* Underground signals carried through common mycelial networks
778 warn neighbouring plants of aphid attack. *Ecol. Lett.* **16**, 835–843 (2013).
779 11. Pieterse, C. M. J., Leon-Reyes, A., Van der Ent, S. & Van Wees, S. C. M. Networking
780 by small-molecule hormones in plant immunity. *Nat. Chem. Biol.* **5**, 308–316
781 (2009).
782 12. Zhou, F. *et al.* Co-incidence of Damage and Microbial Patterns Controls Localized
783 Immune Responses in Roots. *Cell* **180**, 440-453.e18 (2020).
784 13. Orlovskis, Z., Singh, A., Kliot, A., Huang, W. & Hogenhout, S. A. The phytoplasma
785 SAP54 effector acts as a molecular matchmaker for leafhopper vectors by targeting
786 plant MADS-box factor SVP. *eLife* **13**, RP98992 (2025).
787 14. Khashi u Rahman, M., Zhou, X. & Wu, F. The role of root exudates, CMNs, and VOCs
788 in plant–plant interaction. *J. Plant Interact.* **14**, 630–636 (2019).
789 15. Song, Y. Y., Simard, S. W., Carroll, A., Mohn, W. W. & Zeng, R. S. Defoliation of
790 interior Douglas-fir elicits carbon transfer and stress signalling to ponderosa pine
791 neighbors through ectomycorrhizal networks. *Sci. Rep.* **5**, 8495 (2015).

16. Rodriguez-Morelos, V. H., Calonne-Salmon, M., Bremhorst, V., Garcés-Ruiz, M. & Declerck, S. Fungicides With Contrasting Mode of Action Differentially Affect Hyphal Healing Mechanism in Gigaspora sp. and Rhizophagus irregularis. *Front. Plant Sci.* **12**, 642094 (2021).
17. Richter, F., Calonne-Salmon, M., Heijden, M. G. A. van der, Declerck, S. & Stanley, C. E. AMF-SporeChip provides new insights into arbuscular mycorrhizal fungal asymbiotic hyphal growth dynamics at the cellular level. *Lab. Chip* **24**, 1930–1946 (2024).
18. Schütz, L., Saharan, K., Mäder, P., Boller, T. & Mathimaran, N. Rate of hyphal spread of arbuscular mycorrhizal fungi from pigeon pea to finger millet and their contribution to plant growth and nutrient uptake in experimental microcosms. *Appl. Soil Ecol.* **169**, 104156 (2022).
19. Szakiel, A., Pączkowski, C. & Henry, M. Influence of environmental biotic factors on the content of saponins in plants. *Phytochem. Rev.* **10**, 493–502 (2011).
20. Da Silva, P. *et al.* High toxicity and specificity of the saponin 3-GlcA-28-AraRhaxyl-medicagenate, from Medicago truncatula seeds, for Sitophilus oryzae. *BMC Chem. Biol.* **12**, 1–9 (2012).
21. Suzuki, H. *et al.* Lotus japonicus Triterpenoid Profile and Characterization of the CYP716A51 and LjCYP93E1 Genes Involved in Their Biosynthesis In Planta. *Plant Cell Physiol.* **60**, 2496–2509 (2019).
22. D'Addabbo, T. *et al.* Activity of Saponins from Medicago Species against Phytoparasitic Nematodes. *Plants* **9**, 443 (2020).
23. Norvienyeku, J. *et al.* Bayogenin 3-O-cellobioside confers non-cultivar-specific defence against the rice blast fungus Pyricularia oryzae. *Plant Biotechnol. J.* **19**, 589–601 (2021).

817 24. Yan, D.-H. *et al.* Antifungal Activities of Volatile Secondary Metabolites of Four
818 Diaporthe Strains Isolated from Catharanthus roseus. *J. Fungi* **4**, 65 (2018).
819 25. Spaepen, S., Vanderleyden, J. & Remans, R. Indole-3-acetic acid in microbial and
820 microorganism-plant signaling. *FEMS Microbiol. Rev.* **31**, 425–448 (2007).
821 26. McClerklin, S. A. *et al.* Indole-3-acetaldehyde dehydrogenase-dependent auxin
822 synthesis contributes to virulence of Pseudomonas syringae strain DC3000. *PLOS*
823 *Pathog.* **14**, e1006811 (2018).
824 27. Ranocha, P. *et al.* Arabidopsis WAT1 is a vacuolar auxin transport facilitator
825 required for auxin homoeostasis. *Nat. Commun.* **4**, 2625 (2013).
826 28. Fukushima, E. O. *et al.* Combinatorial Biosynthesis of Legume Natural and Rare
827 Triterpenoids in Engineered Yeast. *Plant Cell Physiol.* **54**, 740–749 (2013).
828 29. Qamar, A., Mysore, K. & Senthil-Kumar, M. Role of proline and pyrroline-5-
829 carboxylate metabolism in plant defense against invading pathogens. *Front. Plant*
830 *Sci.* **6**, (2015).
831 30. Siddique, A., Kandpal, G. & Kumar, P. Proline Accumulation and its Defensive Role
832 Under Diverse Stress Condition in Plants: An Overview. *J. Pure Appl. Microbiol.* **12**,
833 1655–1659 (2018).
834 31. Pélissier, R. *et al.* Plant neighbour-modulated susceptibility to pathogens in
835 intraspecific mixtures. *J. Exp. Bot.* **72**, 6570–6580 (2021).
836 32. Alfonso, E. *et al.* Insect eggs trigger systemic acquired resistance against a fungal
837 and an oomycete pathogen. *New Phytol.* **232**, 2491–2505 (2021).
838 33. Erb, M. & Reymond, P. Molecular Interactions Between Plants and Insect
839 Herbivores. *Annu. Rev. Plant Biol.* **70**, 527–557 (2019).
840 34. Chisholm, S. T., Coaker, G., Day, B. & Staskawicz, B. J. Host-Microbe Interactions:
841 Shaping the Evolution of the Plant Immune Response. *Cell* **124**, 803–814 (2006).

842 35. Wenig, M. *et al*. Systemic acquired resistance networks amplify airborne defense
843 cues. *Nat. Commun.* **10**, 3813 (2019).
844 36. Jia, Q. *et al.* Origin and early evolution of the plant terpene synthase family. *Proc.*
845 *Natl. Acad. Sci.* **119**, e2100361119 (2022).
846 37. Jiang, S.-Y., Jin, J., Sarojam, R. & Ramachandran, S. A Comprehensive Survey on the
847 Terpene Synthase Gene Family Provides New Insight into Its Evolutionary Patterns.
848 *Genome Biol. Evol.* **11**, 2078–2098 (2019).
849 38. Wang, Q. *et al.* Expansion and functional divergence of terpene synthase genes in
850 angiosperms: a driving force of terpene diversity. *Hortic. Res.* **12**, uhae272 (2025).
851 39. St-Arnaud, M., Hamel, C., Vimard, B., Caron, M. & Fortin, J. A. Enhanced hyphal
852 growth and spore production of the arbuscular mycorrhizal fungus Glomus
853 intraradices in an in vitro system in the absence of host roots. *Mycol. Res.* **100**, 328–
854 332 (1996).
855 40. Baranski, R. Genetic Transformation of Carrot (Daucus carota) and Other Apiaceae
856 Species. *Transgenic Plant J.* **2**, 18–38 (2008).
857 41. Ron, M. *et al.* Hairy Root Transformation Using Agrobacterium rhizogenes as a Tool
858 for Exploring Cell Type-Specific Gene Expression and Function Using Tomato as a
859 Model. *Plant Physiol.* **166**, 455–469 (2014).
860 42. Vierheilig, H., Coughlan, A. P., Wyss, U. & Piché, Y. Ink and Vinegar, a Simple
861 Staining Technique for Arbuscular-Mycorrhizal Fungi. *Appl. Environ. Microbiol.* **64**,
862 5004–5007 (1998).
863 43. Dobin, A. & Gingeras, T. R. Mapping RNA-seq Reads with STAR. *Curr. Protoc.*
864 *Bioinforma. Ed. Board Andreas Baxevanis Al* **51**, 11.14.1-11.14.19 (2015).
865 44. Kopylova, E., Noé, L. & Touzet, H. SortMeRNA: fast and accurate filtering of
866 ribosomal RNAs in metatranscriptomic data. *Bioinformatics* **28**, 3211–3217 (2012).

45. Ritchie, M. E. *et al.* limma powers differential expression analyses for RNA-sequencing and microarray studies. *Nucleic Acids Res.* **43**, e47 (2015).
46. Tian, T. *et al.* agriGO v2.0: a GO analysis toolkit for the agricultural community, 2017 update. *Nucleic Acids Res.* **45**, W122–W129 (2017).
47. Lohse, M. *et al.* Mercator: a fast and simple web server for genome scale functional annotation of plant sequence data: Mercator: sequence functional annotation server. *Plant Cell Environ.* **37**, 1250–1258 (2014).
48. Thimm, O. *et al.* mapman: a user-driven tool to display genomics data sets onto diagrams of metabolic pathways and other biological processes. *Plant J.* **37**, 914–939 (2004).
49. Usadel, B. *et al.* PageMan: an interactive ontology tool to generate, display, and annotate overview graphs for profiling experiments. *BMC Bioinformatics* **7**, 535 (2006).
50. Usadel, B. *et al.* Extension of the Visualization Tool MapMan to Allow Statistical Analysis of Arrays, Display of Coresponding Genes, and Comparison with Known Responses. *Plant Physiol.* **138**, 1195–1204 (2005).

895 **List of Supplemental tables:**

896 **Supplemental Table 1:** Differentially expressed receiver plant genes (DEGs) in
897 response to sender stimulation by wounding and flg22 in cut and connected CMN
898 treatments.
899 **Tab A**: log2(fold changes) and gene descriptions of 21 809 responder plant DEGs
900 shared in the cut and connected CMN treatment.
901 **Tab B**: log2(fold changes) and gene descriptions of 4885 responder plant DEGs in
902 connected CMN treatment.
903 **Tab C**: log2(fold changes) and gene descriptions of 5698 responder plant DEGs in cut
904 CMN treatment.
905 **Tab D**: log2(fold changes) and gene descriptions of 15 responder plant DEGs which
906 show opposite regulation in cut and connected CMN treatment.
907
908 **Supplemental Table 2:** GO-term enrichment for the 1880 upregulated and 3005
909 downregulated receiver plant DEGs in the connected CMN treatment. Functional
910 enrichment is based on Fisher exact test with Hochberg (FDR) correction using agriGO
911 v2.0. Significantly enriched functions ($p<0.05$; $FDR<0.05$) for each ontology category
912 - biological process, molecular function and cell compartment - are highlighted in bold
913 and coloured.
914 **Tab A**: GO enrichment for the 1880 upregulated DEGs displayed in Figure 1B.
915 Supplemental Figure 4 displays sign. enriched Go-terms corresponding to biological
916 function
917 **Tab B**: GO enrichment for the 3005 downregulated DEGs displayed in Figure 1B.
918 Supplemental Figure 5 displays sign. enriched Go-terms corresponding to biological
919 function and molecular function. Biological function GO terms related to stress
920 response are manually highlighted in yellow
921 **Tab C**: GO-term representation (%) among up- & down-regulated responder plant
922 DEGs and the Medicago truncatula R108 reference genome
923 **Tab D**: List of significantly enriched Mercator4 functional bins containing upregulated
924 receiver DEGs in connected CMN treatment
925 **Tab E**: List of significantly enriched Mercator4 functional bins containing
926 downregulated receiver DEGs in connected CMN treatment
927
928 **Supplemental Table 3:** assignment of plant stress and defence bin for functional
929 enrichment analysis of CMN-mediated receiver plant DEGs
930 **Tab A**: original Mercator4 functional annotation of 39029 Medicago truncatula R108
931 genes based on sequence orthology from all mRNA FASTA files as input.
932 **Tab B**: descriptors of Mercator4 bins that correspond to Plant stress and signalling
933 functions. Only the original Mercator4 output bins from tabA and their corresponding
934 genes are considered. References from the published literature justify the the
935 assignment of bin decriptors to "Defence signalling and response" bin.
936 **Tab C**: Mercator4 BIN contents that are reassigned for the "Defence signalling and
937 response" bin (BINCODE 80)
938 **Tab D**: list of all original Mercator4 functional annotations (tabA) plus the manually
939 reassined "Defence signalling and response" bin (BINCODE 80) from TabC.
940 TabD=TabA+TabC. TabD was used for the enrichment analisis in TabE.

Tab E: Enrichment of Mercator4 functional categories, taking into account the cumulative fold-change of 4885 up-and down-regulated responder DEGs in connected CMN treatment. Analysis performed Mann Whitney U Test (Wilcoxon Rank Sum Test) and Benjamini-Hochberg p-value correction for multiple comparisons to reveal whether the average response (cumulative log2FC) of a BIN is different from the response of all the other BINS. The results are dynamically calculated upon loading of an experiment file with fold changes for a chosen gene list into MapMan tool.
Tab F: List of all 39029 Medicago truncatula R108 genes and subset of Mercator4 annotated functions within the "Defence signalling and response" bin (BINCODE 80), representing 16.9% of total transcripts

Supplemental Table 4: Source data for compound identification using LC-HRMS and HS-GC-MS as well as rCCA and correlation network between transcriptome and metabolome datasets.
Tab A: LC-HRMS data with tentative metabolite id & peak areas used in Figure 3
Tab B: LC-HRMS data calibration with selected standards
Tab C: LC-HRMS data for compound quantification with analytical standards in original & independent samples displayed in Supplemental Figure 8
Tab D: HS-GC-MS data with tentative metabolite id & peak area used in Figure 3
Tab E: HS-GC-MS data calibration with selected standards
Tab F: HS-GC-MS data for compound quantification with analytical standards
Tab G: log2(FC) of compound levels in receivers of WF stimulated vs H2O treated sender signals used to generate volcano plots and heatmap in Figure 3B&C
Tab H: data matrix input for rCCA analysis in Figure 3D; columns with gene and metabolite id; rows - treatments with log2 normalized gene read counts (limma package; CPM counts per million +1 pseudocount) and log2 normalized relative metabolite abundances
Tab I: raw network data obtained with rCCA; from. Nodes describe metabolites; to. nodes describe genes; gene id and corresponding descriptions based on Medicago truncatula R108 reference genome available in https://medicago.toulouse.inrae.fr/MtrunR108_HiC (INRA, Toulouse); FC values based on RNA-seq data wf_connected vs h2o_connected; edge weight is correlation strength based on rCCA for all nodes with correlation >0.7
Tab J: rCCA script in R for correlation network analysis to generate Figure 3D

Supplemental Table 5. Comparison of transcription factors, auxin transporters, P45 and UGT enzyme fold change in receiver from "connected" and "cut" treatments.
Tab A: log2(FC) of upregulated and downregulated DEGs for auxin transporters, auxin response factors, GRAS, MYB transcription factors as well as ethylene response factors in CMN connected receivers
Tab B: log2(FC) of DEGs corresponding to sender signal regulated UDP-glycosyltransferases and cytochrome P450s in "connected" and "cut" treatments
Tab C: log2(FC) of non-DEG (p-adj.>0.05) cytochrome P450 and UGT transcripts in the "connected" and "cut" treatments

Supplemental figures

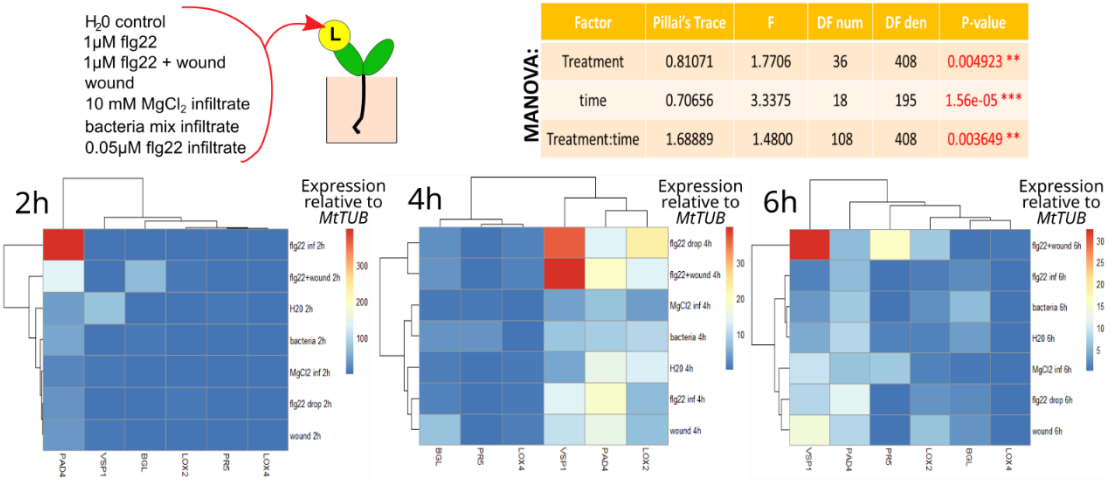

MANOVA:

Factor	Pillai's Trace	F	DF num	DF den	P-value
Treatment	0.81071	1.7706	36	408	0.004923 **
time	0.70656	3.3375	18	195	1.56e-05 ***
Treatment:time	1.68889	1.4800	108	408	0.003649 **

Supplemental Figure 1. Local expression of *Medicago truncatula* immunity markers (*MtPAD4, MtVSP1, MtBGL, MtLOX2, MtLOX4, MtPR5*) relative to *MtTUB* reference gene 2h, 4h and 6h following the application of various stimuli on leaves: mechanical wounding by forceps (3x squeezing leaf blade), 5 µL drop of 1µM flg22, 5 µL drop of dH_2O (control), syringe infiltration of 0.05µM flg22, bacterial mix in 10mM $MgCl_2$ or sterile 10mM $MgCl_2$ as the control. Bacterial mix consisted of live suspension of overnight LB cultures of *Pseudomonas syringae, Dickeya chrysanthemi, Erwinia rhapontici, Pantotea agglomerans* at OD_{660}=0.0005 each. Heatmap displays average expression of 4 independent biological replicates. Each replicate was a pooled sample from two mature stimulated trifoliate leaves from separate plants. 2-factor Multiple Analysis of Variance (MANOVA) indicates significant changes in gene expression over the time-course and differences among the treatments.

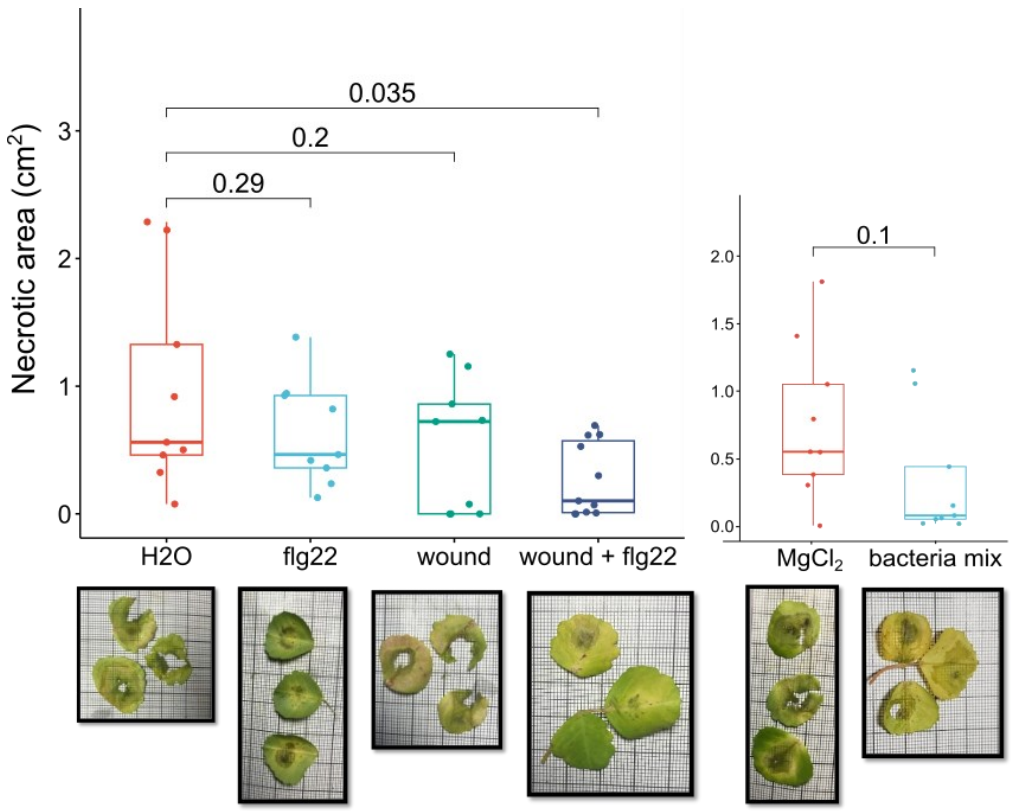

Supplemental Figure 2. Size of *Botrytis cinerea* necrotic lesions (72hpi) on systemic leaves after stimulation of distal leaves with the following treatments: 5µL drop of H_2O (control), 5 µL drop of 1µM flg22, wounding with forceps, wounding + 5 µL drop of 1µM flg22 as well as infiltrations10mM MgCl2 (control), live suspension of *P. syringae, D. chrysanthemi, E. rhapontici, P. agglomerans* at OD_{660}=0.0005 each in 10mM $MgCl_2$. All comparisons were performed at the same time. Box-plots depict distribution of individual data-points and means. ANOVA (F=2,86; p=0.18) suggest significant differences among the treatments and p-values from the Dunnet's two tailed t-test pairwise comparisons are depicted on top of the plots.

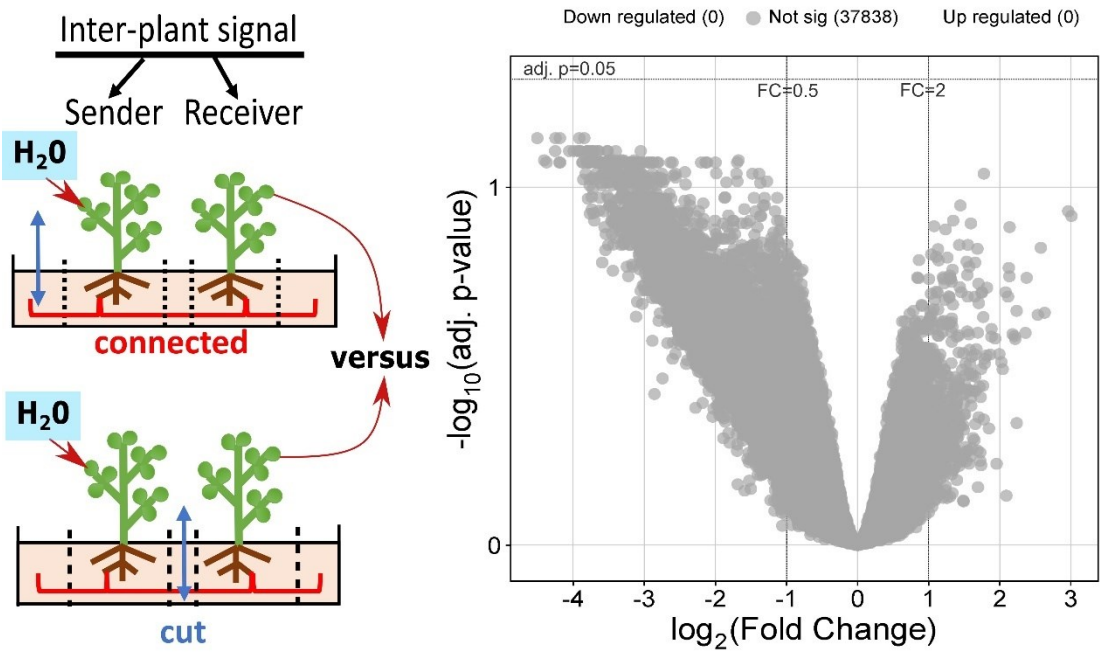

Supplemental Figure 3. No significantly differentially expressed genes (DEGs) were identified when comparing responder plants from CNM connected plant and cut-CNM pots after sender plant treatment with water only. Volcano plot displays $\log_{10}$ of p-adj. and $\log_2$ of fold change for each transcript in the comparison.

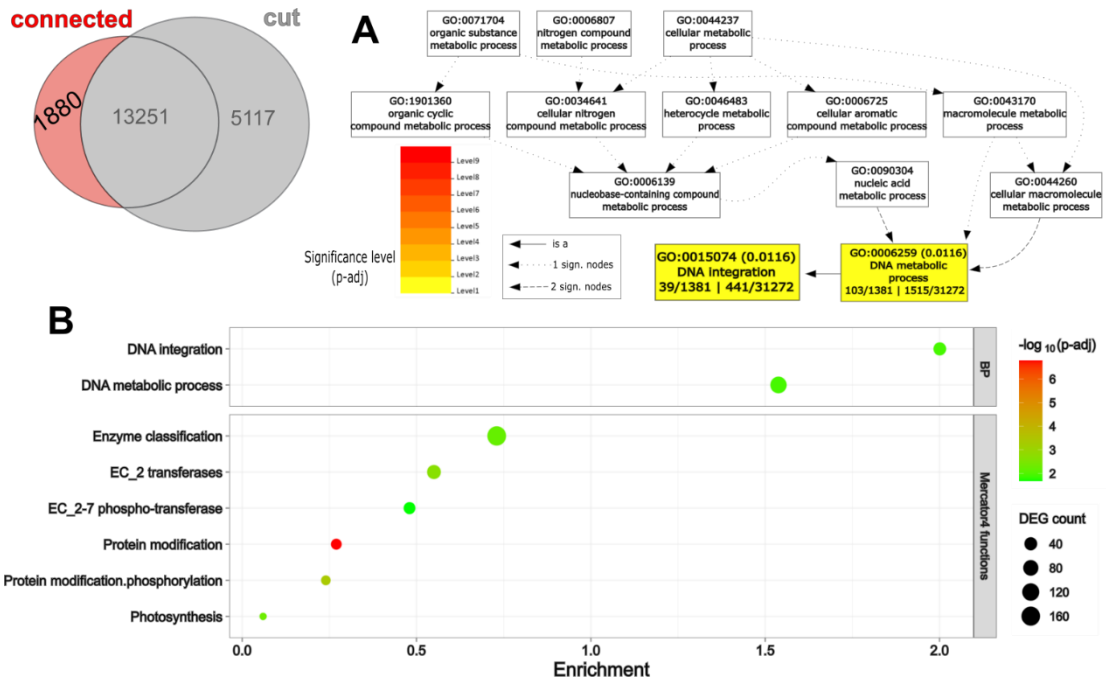

Supplemental Figure 4. Functional enrichment of GO-terms with 1880 upregulated responder plant DEGs in CMN connected plant pots. (**A**) GO-identifiers and their known or inferred hierarchical interactions. Boxes contain colour-coded FDR-corrected p-values, the number DEGs within the GO-term from the query list/total GO-annotations in the query list | total number genes corresponding to the GO-term/ total GO-annotations in the genome. (**B**) Bubble plots depicting the enrichment factor, number of DEGs and log10 normalized FDR-corrected (adj.) p-value for the enrichment significance. Only GO biological functions (BP) and Mercator4 functional predictions with p-adj.<0.05 are displayed. Full list of GO-terms and bins for functional enrichment analysis is available in **Supplemental Table 2 tab-A** (for BP) and **tab D** (for Mercator4 annotation). The BP enrichment is based on the available functional annotations for 73.6% or 1384 out of the 1880 upregulated DEGs (**Supplemental Table 2 tab-C**).

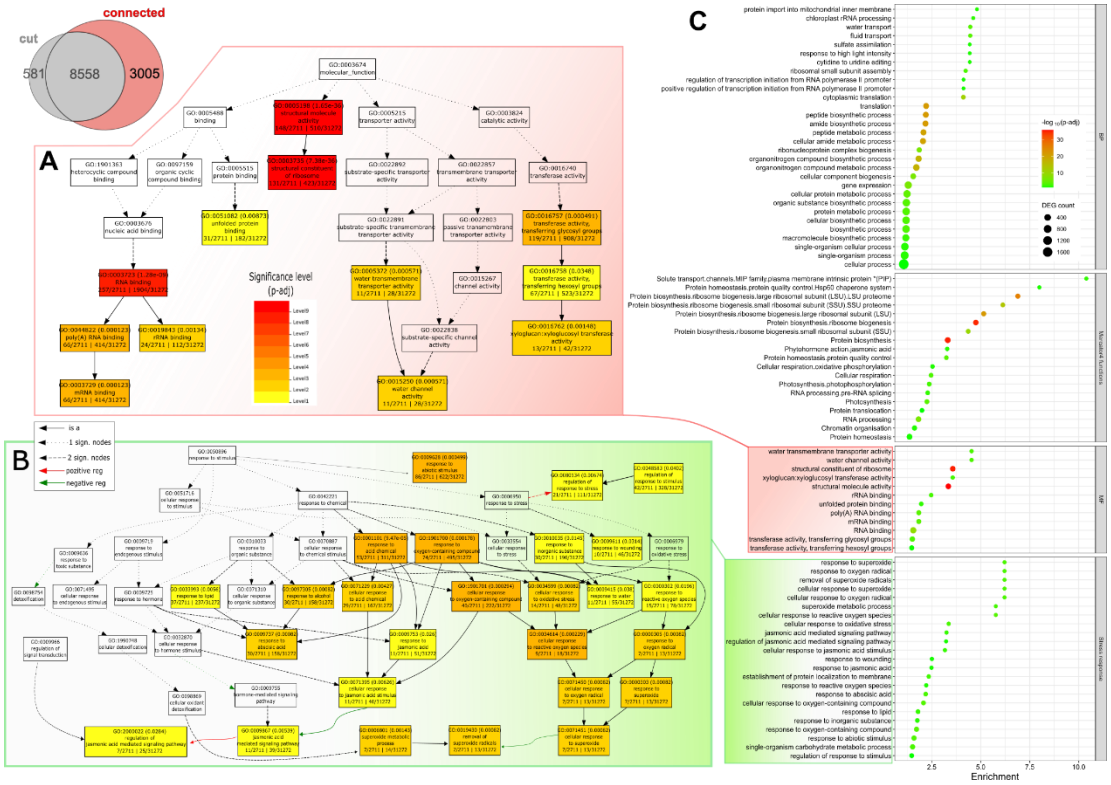

Supplemental Figure 5. Functional enrichment of GO-terms with 3005 downregulated responder plant DEGs in CMN connected plant pots. (**A-B**) GO-identifiers and their known or inferred hierarchical interactions. Boxes contain colour-coded FDR-corrected p-values, the number DEGs within the GO-term from the query list/total GO-annotations in the query list | total number genes corresponding to the GO-term/ total GO-annotations in the genome. Different arrow types indicate GO-terms associated to 1 or 2 other significant enriched functions as well as known positive or negative regulation between genes within the associated GO-term. (**A**) Enriched GO-identifiers for molecular functions (MF) related to RNA binding and ribosome functions. (**B**) Enriched GO-identifiers for biological processes related to ROS metabolism, response to stimuli and jasmonic acid, collectively displayed under Stress response cluster. (**C**) Bubble plots depicting the enrichment factor, number of DEGs and log10 normalized FDR-corrected (adj.) p-value for the enrichment significance. For brevity the plot displays the top 30 most sign. Enriched GO biological functions (BP subpanel). All GO-terms with p-adj.<0.05 are displayed in the Stress response, MF and Mercator4 subpanels. Full list of GO-term descriptor for enrichment analysis is available in **Supplemental Table 2 tab-B** (for BP and MF) and **tab E** (for Mercator4 annotation). The displayed **Stress response** category represents a subset of BP GO-terms that were manually assigned to this category based on the description semantics and are fully listed in **Supplemental Table 2 tab-B.** The BP and MF enrichment is based on the available functional annotations for 90.3% or 2713 out of the 3005 DEGs (**Supplemental Table 2 tab-C**).

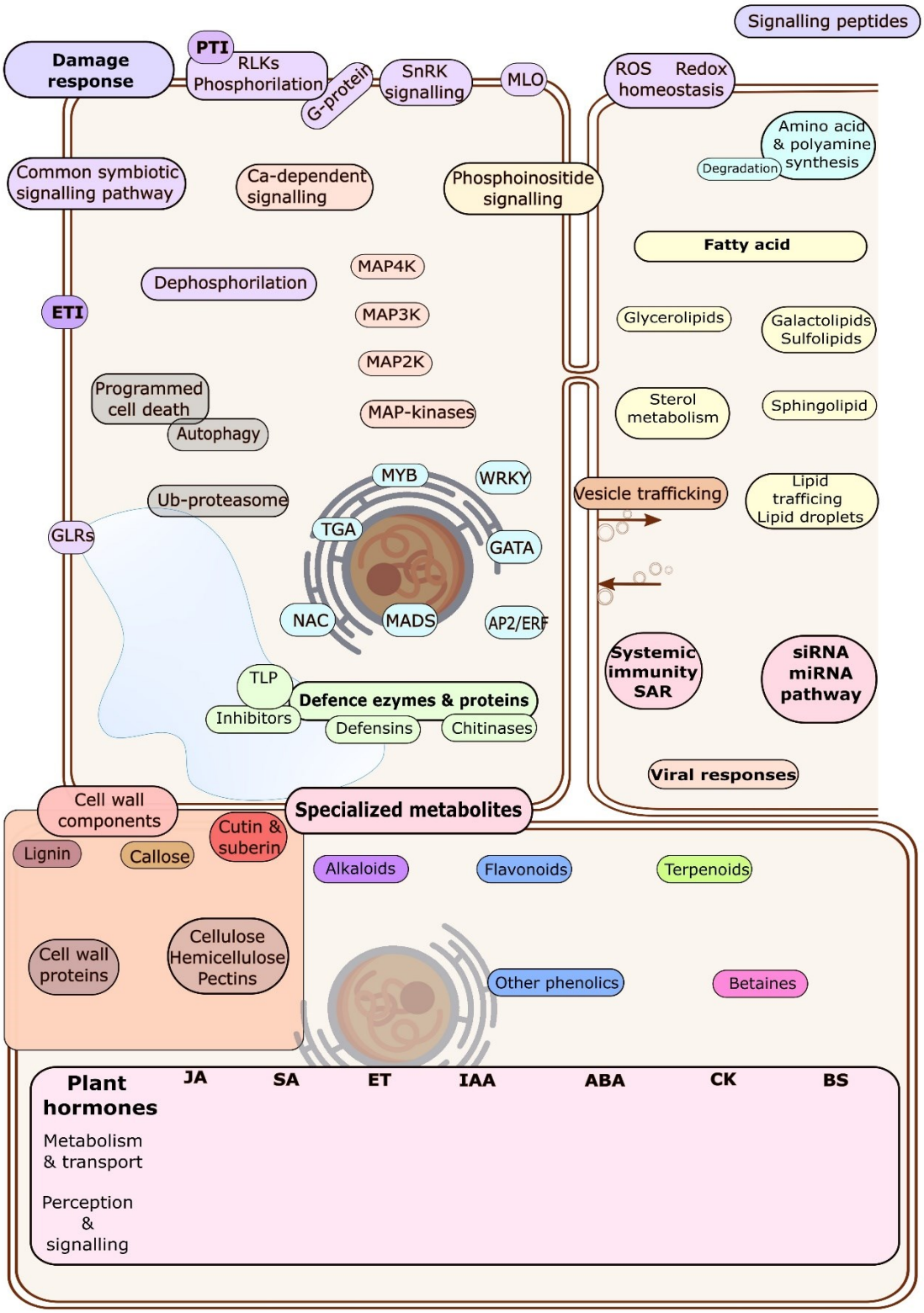

Supplemental figure 6. Image file for manually curated ''Defence signalling & response'' category to display fold change of genes corresponding to bins listed in **Supplemental Table 3 tab-C.**

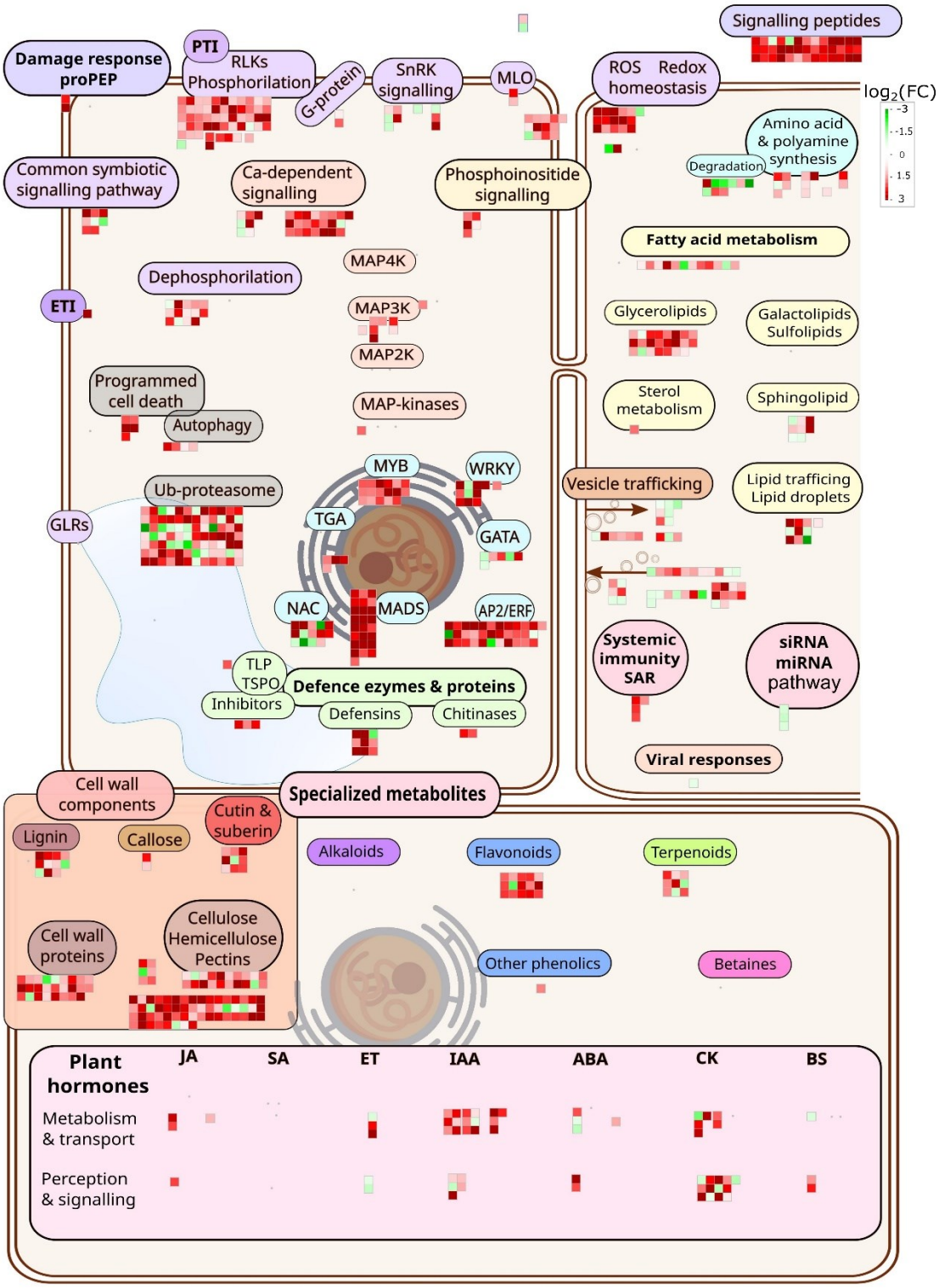

Supplemental figure 7. Plant ''Defence signalling & response'' pathways genes are upregulated in receivers with cut CMN. Log2 (transcript fold) changes of plant functions encoded by up- (red) and down-regulated (green) DEGs in receivers of wound and flg22 signals compared to H_2O controls.

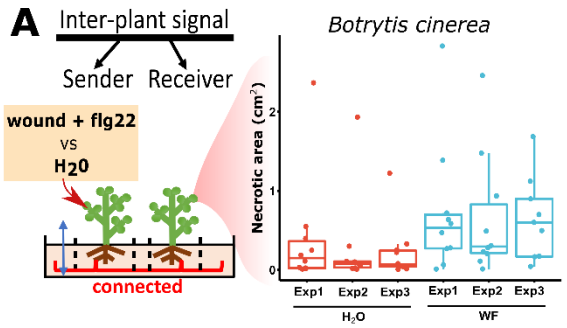

Botrytis cinerea Connected CMN	Treatment group	Shapiro-Wilk normality test	2-tailed t-test	Mann-Whitney U test		
Experiment 1	control	W = 0.59577, p = 2.252e-05	na	W = 24, p = 0.03129	Linear mixed model fit by REML ['lmerModLmerTest'] % x ~ y + (1 | r) x-lesion size y-sender treatment r-repeated experiments	
	WF	W = 0.76616, p = 0.005616				
Experiment 2	control	W = 0.5807, p = 3.259e-05	na	W = 33, p = 0.2118		
	WF	W = 0.77536, p = 0.007269				
Experiment 3	control	W = 0.47598, p = 1.904e-06	na	W = 17, p = 0.02462	Random effect by repeated experiments Likelihood Ratio Test	Fixed effect by Sender stimulus (control vs WF)
	WF	W = 0.93581, p = 0.5385				
Pooled 3 experiments	control	W = 0.535, p = 8.95e-9	na	W = 220.0, p = 0.0007	LRT <0.0001, p = 1.0 (Chisq)	F = 5.6603, p = 0.02066
	WF	W = 0.813, p = 0.00014				

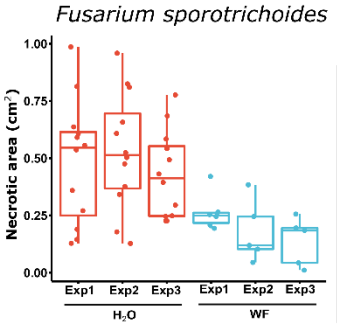

Fusarium sporotrichoides Connected CMN	Treatment group	Shapiro-Wilk normality test	2-tailed t-test	Mann-Whitney U test		
Experiment 1	control	W = 0.91923, p = 0.2449	t = 2.2044, p = 0.04157	na	Linear mixed model fit by REML ['lmerModLmerTest'] % x ~ y + (1 | r) x-lesion size y-sender treatment r-repeated experiments	
	WF	W = 0.7976, p = 0.05592				
Experiment 2	control	W = 0.94193, p = 0.5235	t = 2.3694, p = 0.03166	na		
	WF	W = 0.91455, p = 0.4954				
Experiment 3	control	W = 0.97421, p = 0.9495	t = 3.2788, p = 0.005075	na	Random effect by repeated experiments Likelihood Ratio Test	Fixed effect by Sender stimulus (control vs WF)
	WF	W = 0.89575, p = 0.3868				
Pooled 3 experiments	control	W = 0.962, p = 0.233	t = 4.621, p = 2.63xe-5	na	LRT = 3.3751e-14, p = 1.0 (Chisq)	F = 21.355, p = 2.629e-05
	WF	W = 0.951, p = 0.5				

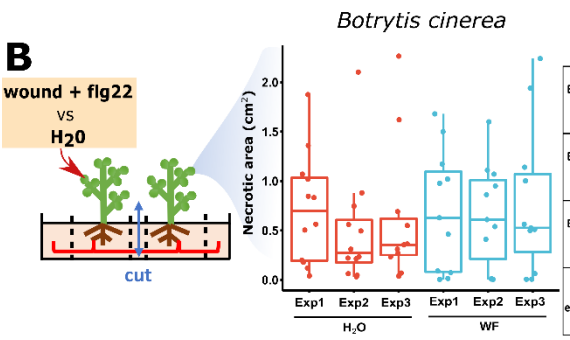

Botrytis cinerea Cut CMN	Treatment group	Shapiro-Wilk normality test	2-tailed t-test	Mann-Whitney U test		
Experiment 1	control	W = 0.80505, p = 0.0107	na	W = 64, p = 0.9279	Linear mixed model fit by REML ['lmerModLmerTest'] % x ~ y + (1 | r) x-lesion size y-sender treatment r-repeated experiments	
	WF	W = 0.90332, p = 0.2028				
Experiment 2	control	W = 0.93712, p = 0.4617	t = 0.2878, p = 0.7763	na		
	WF	W = 0.93427, p = 0.4556				
Experiment 3	control	W = 0.74729, p = 0.002504	na	W = 51, p = 0.3793	Random effect by repeated experiments Likelihood Ratio Test	Fixed effect by Sender stimulus (control vs WF)
	WF	W = 0.86871, p = 0.07462				
Pooled 3 experiments	control	W = 0.84323, p = 0.0001335	na	W = 558.5, p = 0.6741	LRT = 2.8422e-14, p = 1.0 (Chisq)	F = 0.3496, p = 0.5563
	WF	W = 0.91345, p = 0.01212				

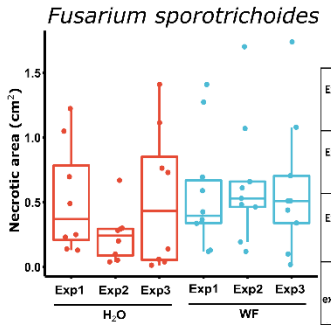

Fusarium sporotrichoides Cut CMN	Treatment group	Shapiro-Wilk normality test	2-tailed t-test	Mann-Whitney U test		
Experiment 1	control	W = 0.87739, p = 0.1474	t = -0.26405, p = 0.7949	na	Linear mixed model fit by REML ['lmerModLmerTest'] % x ~ y + (1 | r) x-lesion size y-sender treatment r-repeated experiments	
	WF	W = 0.84384, p = 0.04905				
Experiment 2	control	W = 0.86585, p = 0.1372	t = -0.54953, p = 0.5907	na		
	WF	W = 0.86664, p = 0.1131				
Experiment 3	control	W = 0.85667, p = 0.1112	t = -1.8179, p = 0.0891	na	Random effect by repeated experiments Likelihood Ratio Test	Fixed effect by Sender stimulus (control vs WF)
	WF	W = 0.88863, p = 0.1931				
Pooled 3 experiments	control	W = 0.85205, p = 0.001926	na	W = 256.5, p = 0.09747	LRT <0.0001, p = 1.0 (Chisq)	F = 2.089, p = 0.1545
	WF	W = 0.87513, p = 0.00314				

Supplemental figure 8. Size of necrotic lesions on *Mediago truncatula* receiver leaves 72h after inoculation with *Botrytis cinerea* and *Fusarium sporotichoides* in CMN-connected (A) and cut CMN treatments (B). Experiments in panel A and B were performed independently three times, each with 10-11 biological replicates. Line indicates the median, boxes represent the interquartile range (IQR), whiskers - variance within 1.5xIQR. Table displays test-statistics for each individual experiment as well as the pooled data represented in the **Figure 4**. Mann-Whitney U-test was performed where data deviate from normal distribution after Shapiro-Wilk test. Two-tailed t-test was performed on normally distributed data. Pooled data were analysed using linear mixed model (lmer). Results did not differ among repeated experiments for any of the treatments as demonstrated by Likelihood Ratio Test (LRT) and non-significant p-values for the associated Chi-square test. Only sender plant treatment displayed significant effect on receiver lesion size in the connected CMN treatment (**A**).

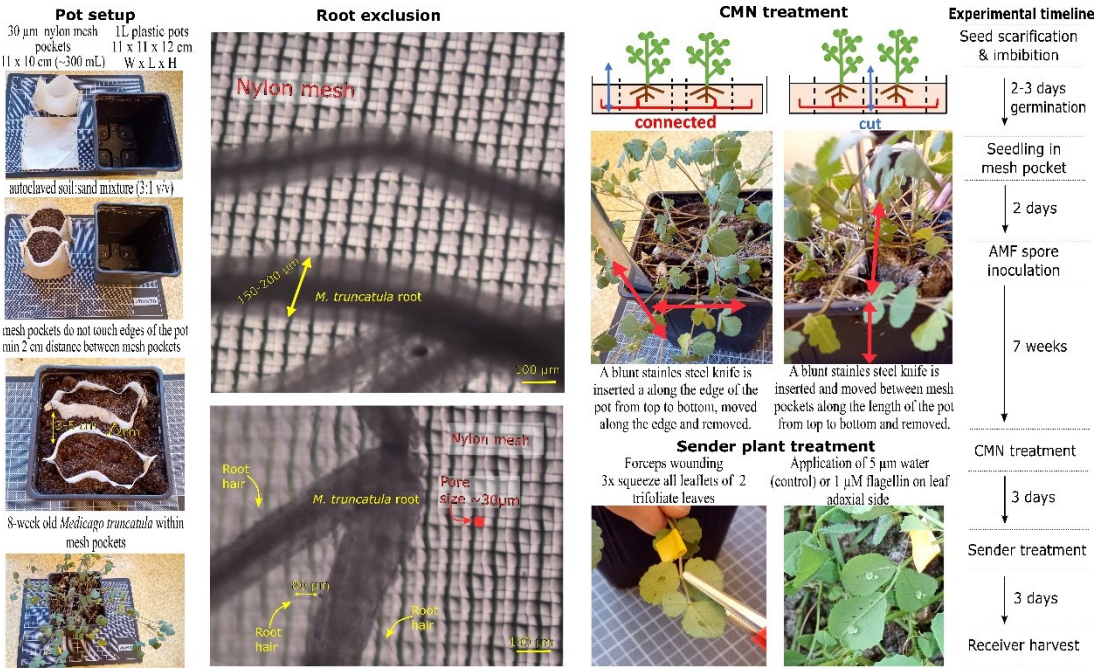

Supplemental figure 9. Visual representation of the experimental setup and treatments. The distance between the mesh pockets is >2cm in the middle of the pots and increases towards the edges (3-5cm) due to the geometry of soil-filled mesh pockets. *Medicago truncatula* fine roots are 150-200 µm in diameter and cannot penetrate through the 30 µm mesh or be injured during the knife treatment of CMN. The root hairs may penetrate through the pore size but due to their short length (50-80 µm) and the distance between the plants (>2cm) they cannot make physical inter-plant contact.

A

Gene ID	WF_con vs H2O con	WF_cut vs H2O cut	FC Difference
MedtrR108_hic.HiC_scaffold_1.85.gene	3.84	3.73	-2.06
MedtrR108_hic.HiC_scaffold_3.5199.gene	3.68	1.20	-2.60
MedtrR108_hic.HiC_scaffold_3.5376.gene	3.66	1.48	2.4
MedtrR108_hic.HiC_scaffold_7.156.gene	3.77	1.58	2.16
MedtrR108_hic.HiC_scaffold_2.2804.gene	3.77	1.30	-2.08
MedtrR108_hic.HiC_scaffold_7.2087.gene	3.77	1.37	1.75
MedtrR108_hic.HiC_scaffold_2.1243.gene	3.68	2.46	1.42
MedtrR108_hic.HiC_scaffold_6.1819.gene	3.76	2.31	1.16
MedtrR108_hic.HiC_scaffold_2.2808.gene	3.72	1.59	0.81
MedtrR108_hic.HiC_scaffold_4.3247.gene	3.41	3.1	0.61
MedtrR108_hic.HiC_scaffold_2.4166.gene	2.36	5.29	-2.90
MedtrR108_hic.HiC_scaffold_3.140.gene	1.68	5.17	-3.49
MedtrR108_hic.HiC_scaffold_1.2855.gene	1.62	5.19	-3.27
MedtrR108_hic.HiC_scaffold_7.2898.gene	1.60	5.25	-3.6
MedtrR108_hic.HiC_scaffold_1.1607.gene	1.47	5.12	-3.7
MedtrR108_hic.HiC_scaffold_2.3809.gene	1.28	5.13	-3.85
MedtrR108_hic.HiC_scaffold_2.3487.gene	1.42	5.34	-3.96
MedtrR108_hic.HiC_scaffold_4.595.gene	1.21	5.18	-3.97
MedtrR108_hic.HiC_scaffold_8.3605.gene	1.36	5.36	-3.99
MedtrR108_hic.HiC_scaffold_6.1167.gene	1.16	5.2	-4.04

Gene ID	WF_con vs H2O con	WF_cut vs H2O cut	FC Difference
MedtrR108_hic.HiC_scaffold_612.1.gene	-1.65	-4.87	-2.76
MedtrR108_hic.HiC_scaffold_5.3781.gene	-1.67	-4.72	-2.55
MedtrR108_hic.HiC_scaffold_4.954.gene	-1.62	-4.21	-2.4
MedtrR108_hic.HiC_scaffold_5.2631.gene	-2.17	-4.9	-2.39
MedtrR108_hic.HiC_scaffold_3.2548.gene	-2.81	-4.82	-2.01
MedtrR108_hic.HiC_scaffold_2.863.gene	-2.82	-4.34	-1.51
MedtrR108_hic.HiC_scaffold_2.274.gene	-4.19	-5.28	0.53
MedtrR108_hic.HiC_scaffold_7.2364.gene	-4.29	-4.93	0.36
MedtrR108_hic.HiC_scaffold_8.1361.gene	-4.19	-4.76	-0.91
MedtrR108_hic.HiC_scaffold_8.1361.gene	-4.27	-4.76	-0.91
MedtrR108_hic.HiC_scaffold_7.100.gene	-3.11	-2.99	2.72
MedtrR108_hic.HiC_scaffold_6.361.gene	-4.28	-3.01	-3.75
MedtrR108_hic.HiC_scaffold_1.3113.gene	-4.49	-2.93	-3.75
MedtrR108_hic.HiC_scaffold_6.360.gene	-4.65	-2.69	3.96
MedtrR108_hic.HiC_scaffold_7.2979.gene	-1.1	-4.93	-3.85
MedtrR108_hic.HiC_scaffold_6.2833.gene	-4.8	2.56	-8.34
MedtrR108_hic.HiC_scaffold_6.824.gene	-3.74	-2.42	3.32
MedtrR108_hic.HiC_scaffold_4.2775.gene	-3.91	-3.69	2.22
MedtrR108_hic.HiC_scaffold_1.619.gene	-4.46	-3.36	-8.97
MedtrR108_hic.HiC_scaffold_8.692.gene	-4.65	-1	-6.35

B

Gene ID	WF_con vs H2O con	WF_cut vs H2O cut	WF_con vs H2O con after pathogen	WF_cut vs H2O cut after pathogen
MedtrR108_hic.HiC_scaffold_4.1000.gene	0.036	-0.032	0.024	0.112
MedtrR108_hic.HiC_scaffold_1.3531.gene	0.032	-0.006	0.051	-0.131
MedtrR108_hic.HiC_scaffold_1.1153.gene	-0.040	0.065	0.019	-0.101
MedtrR108_hic.HiC_scaffold_3.3028.gene	0.034	-0.032	-0.182	0.045
MedtrR108_hic.HiC_scaffold_7.2914.gene	-0.028	0.018	-0.009	0.218
MedtrR108_hic.HiC_scaffold_2.2705.gene	-0.009	-0.083	-0.123	0.048
MedtrR108_hic.HiC_scaffold_7.324.gene	-0.082	0.007	-0.066	-0.069
MedtrR108_hic.HiC_scaffold_2.2950.gene	0.029	-0.031	-0.218	-0.043
MedtrR108_hic.HiC_scaffold_3.3836.gene	-0.015	0.067	-0.088	-0.158
MedtrR108_hic.HiC_scaffold_6.1810.gene	0.017	-0.022	0.212	-0.080
MedtrR108_hic.HiC_scaffold_6.2721.gene	0.066	0.048	-0.181	-0.062
MedtrR108_hic.HiC_scaffold_4.4731.gene	0.010	0.094	-0.078	-0.178
MedtrR108_hic.HiC_scaffold_7.4223.gene	0.030	0.070	-0.066	-0.199
MedtrR108_hic.HiC_scaffold_2.4209.gene	0.092	-0.019	0.203	0.032
MedtrR108_hic.HiC_scaffold_1.4070.gene	0.017	0.085	-0.072	0.198
MedtrR108_hic.HiC_scaffold_1.817.gene	0.009	0.093	0.290	-0.022
MedtrR108_hic.HiC_scaffold_5.1824.gene	-0.031	-0.022	-0.312	0.033
MedtrR108_hic.HiC_scaffold_8.1977.gene	-0.092	-0.044	0.083	-0.180
MedtrR108_hic.HiC_scaffold_7.3435.gene	-0.011	0.068	-0.011	0.291

C

Primer efficiency (E%) = $\left(10^{\frac{-1}{slope}} - 1\right) \times 100$

relative expression = $\frac{\sqrt{E_{ref1}^{Ct(ref1)} \times E_{ref2}^{Ct(ref2)}}}{E_{test}^{Ct(test)}}$

Correlation between

rt-qPCR of test genes
log2 (relative expression)
&
RNAseq of selected genes
cmps = $\log_2$ (counts per million)

D

Nr.	Gene_ID	Locus_tag	Description	Primer name	Primer sequence (5' -> 3')	Predicted product lenght (bp)	Tm	GC %	Self complementarity	Self 3' complementarity	Test / reference	Primer amplification efficiency E
1	MedtrR108_hic.HiC_scaffold_1.85.gene	MtrunR108HiC_000085	Putative protein - F-box protein interaction domain protein	PP1	F_CAGAGGGCCAACCTTCTCAG R_TTCTTCCAAAGGCCGAGCAT	207	60,04 59,96	60 50	4 4	3 2	test	107.1605204
2	MedtrR108_hic.HiC_scaffold_3.5376.gene	MtrunR108HiC_015574	Putative protein - transmembrane protein	PP2	F_CTCCCGTTCAGCATCATTGC R_TGGGTAGCCCTATAGCCAGAA	185	59,62 59,78	55 52,38	3 6	3 0	test	99.94584797
3	MedtrR108_hic.HiC_scaffold_3.5199.gene	MtrunR108HiC_015397	Putative protein - retrovirus-related Pol polyprotein from transposon TNT 1-94	PP3	F_CCTCCGGAAAATGTTGAACCAA R_AGGCATAGGAACCAAATCCCA	229	59,37 59,07	45,45 47,62	6 3	3 0	test	No amplification
4	MedtrR108_hic.HiC_scaffold_6.1167.gene	MtrunR108HiC_026783	Putative premnaspirodiene oxygenase - cytochrome P450 71D11	PPO	F_TGGAGCTGTTGAGTACGAACC R_GTAGCCAATGCTGTGAGGGA	270	60 59,75	52,38 55	4 3	2 0	test	96.42761402
5	MedtrR108_hic.HiC_scaffold_8.692.gene	MtrunR108HiC_034524	Putative germin, rmlC-like cupin domain superfamily, rmlC-like jelly roll, germin, manganese binding - auxin-binding protein ABP19a	ABP19	F_GGTCTCTCTGCAGCAAGGTT R_CTCTTACCAGCAGTGGCTTGA	215	59,96 60	55 52,38	6 3	2 1	test	96.88509494
6	MedtrR108_hic.HiC_scaffold_1.619.gene	MtrunR108HiC_000619	Non-specific Lipid Transfer Protein - 14 kDa proline-rich protein DC2.15-like	DC2	F_ACCAACTCCATCACCTAAGCC R_AGCAATGCACAACACTTGCTT	207	59,72 59,86	52,38 42,86	3 5	1 3	test	97.52618252
7	MedtrR108_hic.HiC_scaffold_4.2775.gene	MtrunR108HiC_018446	Late Anther Tomato52/Pollen Ole e 1 Allergen and Extensin - proline-rich protein 4	PrP4	F_CTAGCCAGGCTTTCTCAGGG R_GCAGCAGCAGTACTTAGGGT	277	59,82 59,75	60 55	7 6	1 2	test	108.7302414
8	MedtrR108_hic.HiC_scaffold_6.824.gene	MtrunR108HiC_026440	Putative chitinase - basic endochitinase	PC	F_ACATGCAACACGGGTCTCTT R_TGGGTGGGTTACAATGACCAG	106	59,89 59,93	50 52,38	4 3	2 1	test	99.48355391
9	MedtrR108_hic.HiC_scaffold_6.2833.gene	MtrunR108HiC_028449	Putative leucine-rich repeat domain superfamily - leucine-rich repeat extensin-like protein 4	LP4	F_AATGTTTTCTGTGCACCCGC R_CGGAGAACAACCTCCGGAAA	251	59,97 59,97	50 55	6 6	2 2	test	97.75451912
10	MedtrR108_hic.HiC_scaffold_7.2979.gene	MtrunR108HiC_031735	Putative transcription factor NAM family - NAC transcription factor 47	NAC47	F_ATTGCCATGTGGAGGAGGAC R_CGGCATAGCACCCAATCATC	192	59,74 59,12	55 55	4 3	1 1	test	98.67730771
11	MedtrR108_hic.HiC_scaffold_2.3333.gene	MtrunR108HiC_008637	NA - calcium-binding protein PBP1	PBP1	F_AAGCTTGGTGGGGATGGATT R_TCTTGTAACCCAAGCAAAGCTG	125	59,29 59,38	50 45,45	6 4	1 2	test	105.2254875
12	MedtrR108_hic.HiC_scaffold_7.324.gene	MtrunR108HiC_029080	exocyst complex component EXO70E2	EXO70	F_ATTCGGACGAGGTTGGTTCC R_CGGACTCGTATCAGGTGACG	272	60,04 59,97	55 60	4 4	2 3	reference	99.54860257
13	MedtrR108_hic.HiC_scaffold_1.3531.gene	MtrunR108HiC_003531	RNA-binding protein 28	RNA-BP28	F_AGAACCAAAGGAAGAAGAAGTGA R_CACACAGTGCCGATTTCTCTG	216	57,63 59,54	39,13 52,38	2 5	1 1	reference	92.36201716

E

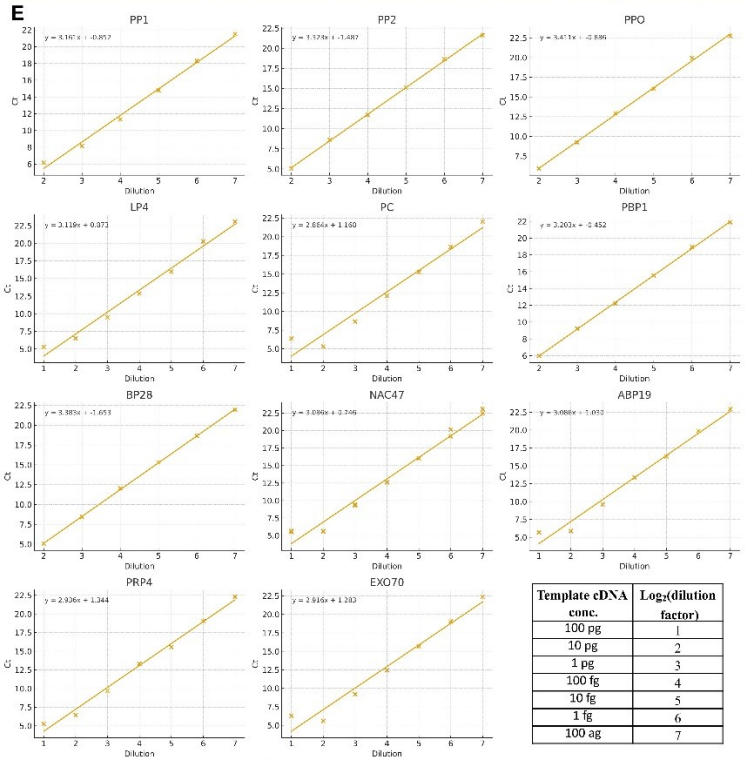

Template cDNA conc.	Log_2(dilution factor)
100 pg	1
10 pg	2
1 pg	3
100 fg	4
10 fg	5
1 fg	6
100 ag	7

F

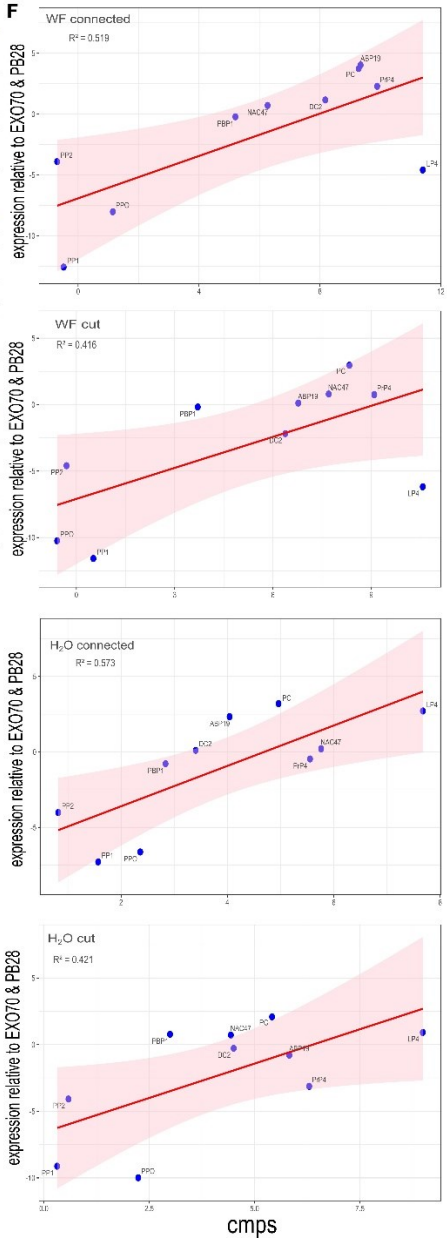

G

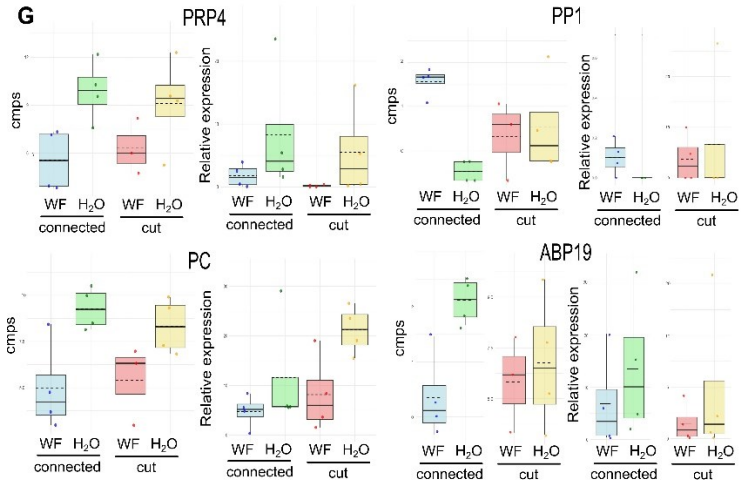

1126 **Supplemental figure 10. Correlation of gene expression data from RNA-seq experiment**
1127 **and an independent sample set. (A)** Test genes were selected based on the highest log2FC in
1128 signal receivers from wound and flg22 (WF) treated plants with intact or cut CMN as well as
1129 the largest relative differences between the "connected" and "cut" treatments. **(B)** Candidate
1130 reference genes were selected among the genes with the lowest FC and no sign. FC among any
1131 of the treatments. Selected references were EXO70 and RNA-BP28. **(C)** Analysis pipeline and
1132 equations used for calculating the primer efficiency and relative expression. **(D)** Full list of the
1133 selected test and reference gene primers and gene descriptors. Primer efficiency was first
1134 calculated using a dilution series of gel-purified cDNA amplicons displayed in (**E**). Relative
1135 expression was calculated as the geometric mean of the amplification of two reference genes
1136 divided by the amplification of a test gene **(C)**. The correlation between the relative expression
1137 of selected targets from independent samples by rt-qPCR and RNA-seq is depicted in panel **(F).**
1138 The expression pattern of representative set of test genes in the "connected" and "cut" systems
1139 after WF and H_2O treatments is similar in RNA-seq and qPCR analysis from independent
1140 samples. CMPS (plural) refers to counts per million from *limma* package output files.

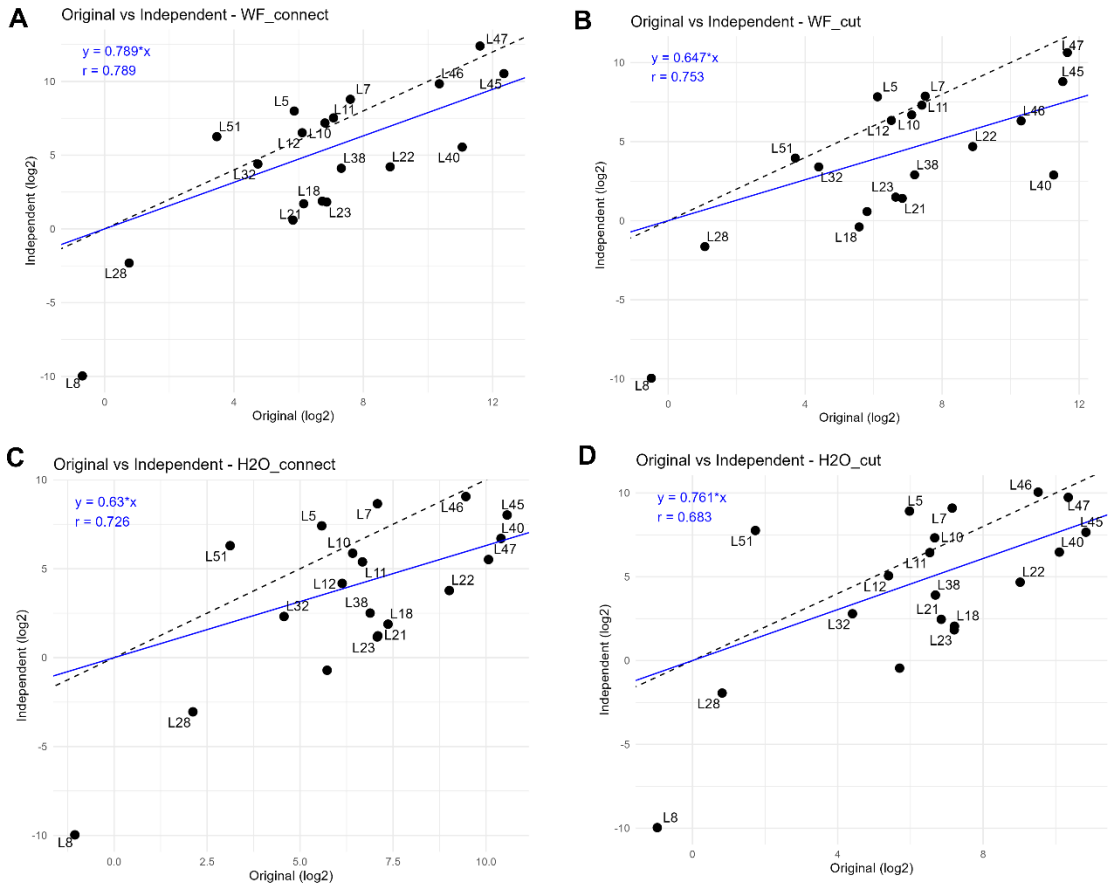

ID	Compound
L5	Proline
L7	(S)-Homostachydrine
L8	Tyrosine
L10	Leucine/Isoleucine (Summ)
L11	Phenylalanine
L12	Tryptophane
L18	Apigenin 7-O-diglucuronide
L21	Apigenin 7-O-glucuronide
L22	ApigeninFerGlcAGlcA*
L23	Apigenin CouGlcAGlcA
L24	Apigenin 7-Glucosyl-(1->2)-glucuronide-4'-glucuronide
L28	ApigeninFerGlcAGlcAGlcA
L32	Jasmonic acid
L38	Malonyl-dHex-Hex-HexA-Soyasapogenol B (Pisumsaponin I)
L40	3-Hex-Hex-28-Ara-Rha-(Api)-Xyl-medicagenic acid I
L45	3-Hex-Hex-28-Ara-Rha-(Api)-Xyl-medicagenic acid II
L46	Acetylsoyasaponin A3
L47	3-Hex-Hex-28-Ara-Rha-(Api)-Xyl-medicagenic acid III
L51	Hex-Hex-soyasapogenol E

Supplemental figure 11. Correlation of metabolite levels from two independent repeated experiments. The ''original'' sample data are presented in Figure 3. The ''independent'' samples were obtained from an independent repeated experiment. Comparisons between the ''original'' and ''independent'' samples include intact **(A)** or cut **(B)** CMN between receivers and wound and flg22 (WF) treated senders as well as intact **(C)** or cut **(D)** CMN between receivers and water-treated senders. Dashed black line corresponds to perfect correlation between ''original'' and ''independent'' samples. Blue line and the equation indicate fitted regression line for the correspondence of both datasets along with Pearson correlation (r). The compound quantities (µg/g FW) were determined using the available standards and available in **Supplemental Table 4 tab-C**.

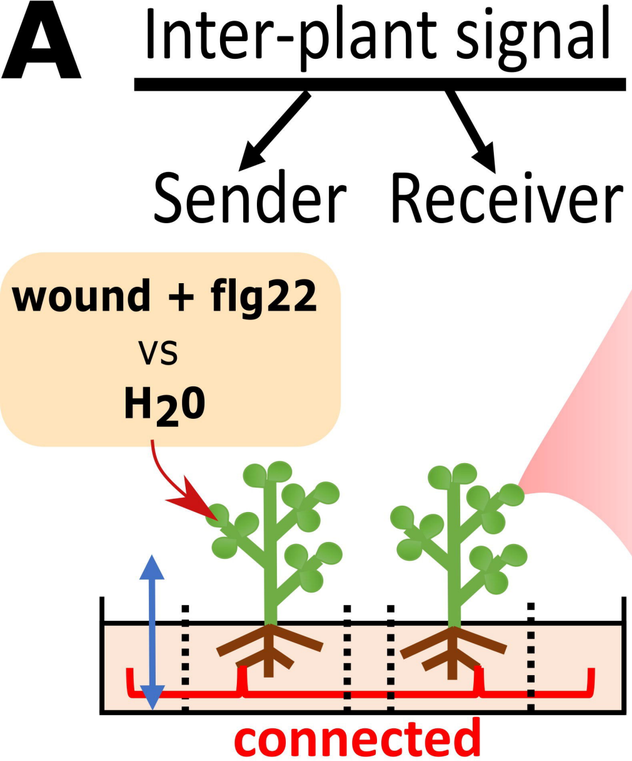

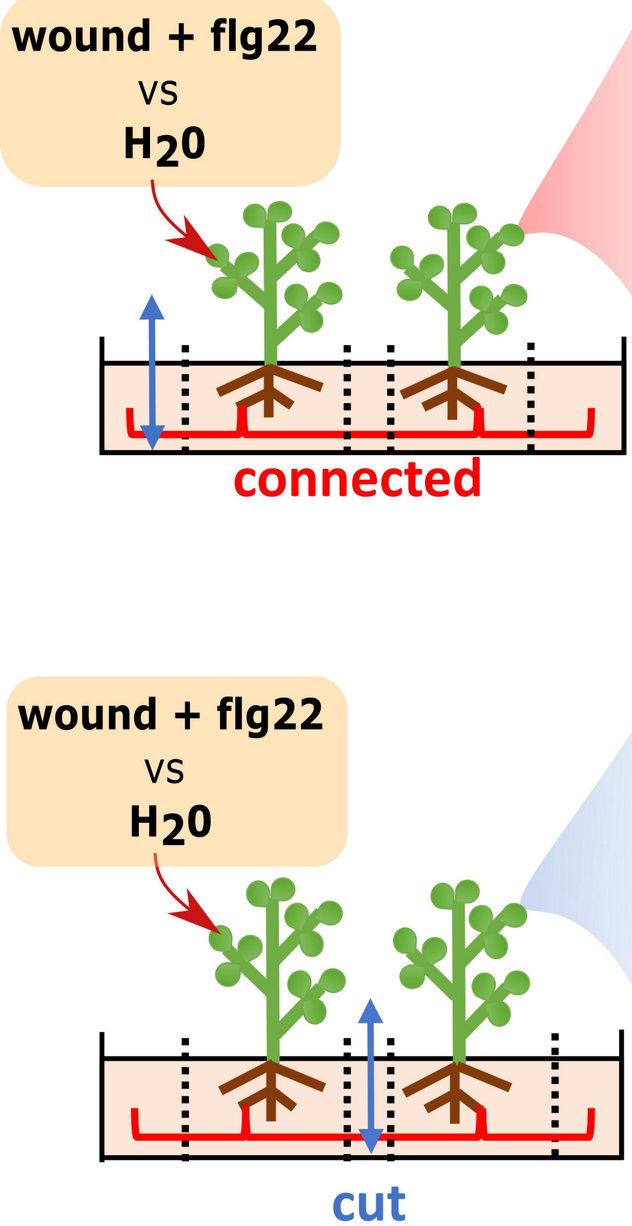

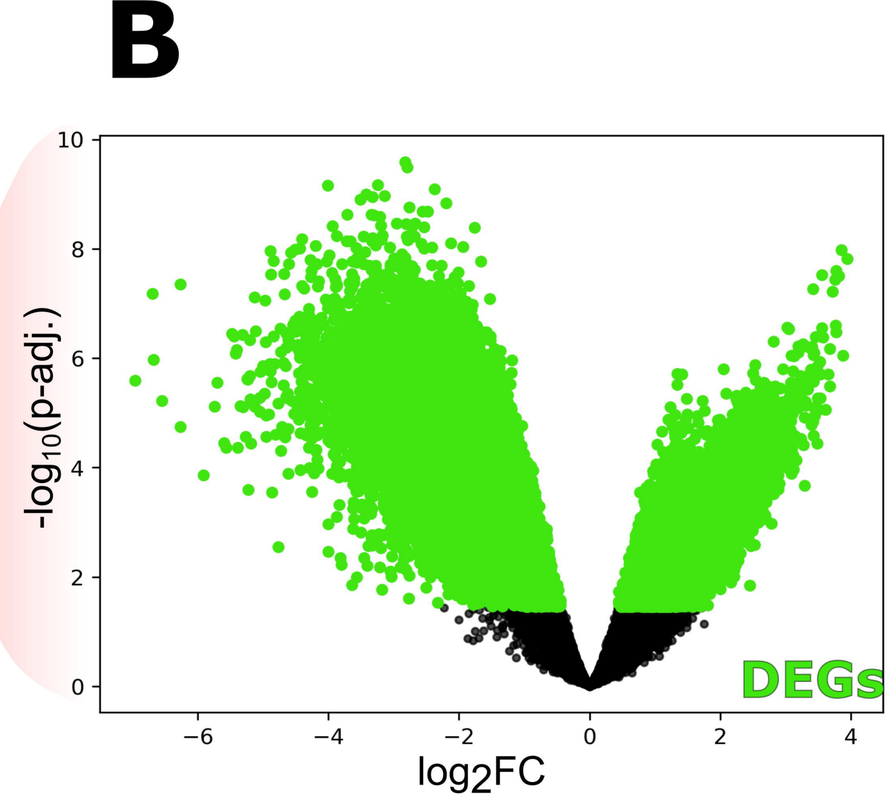

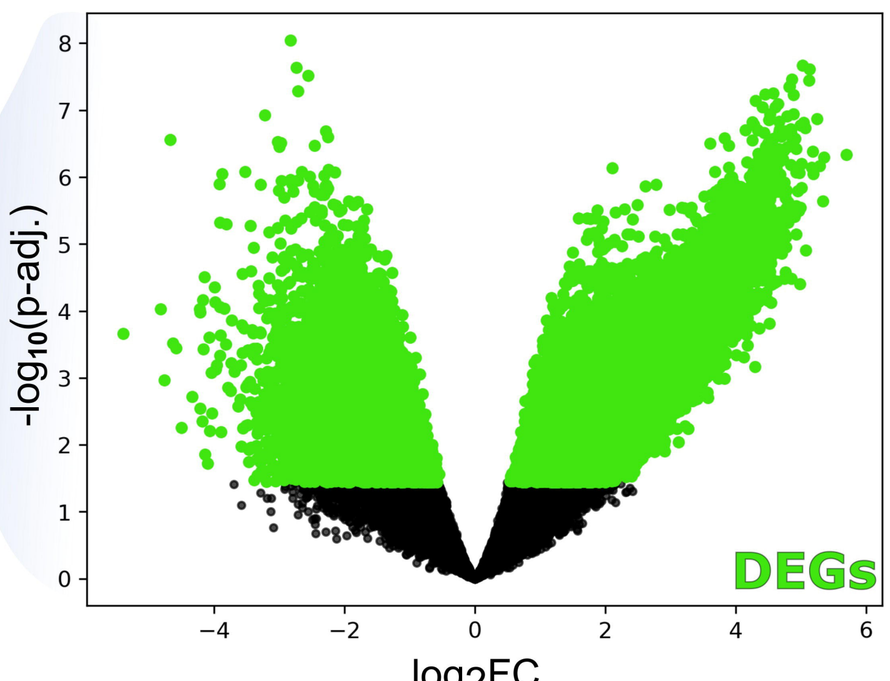

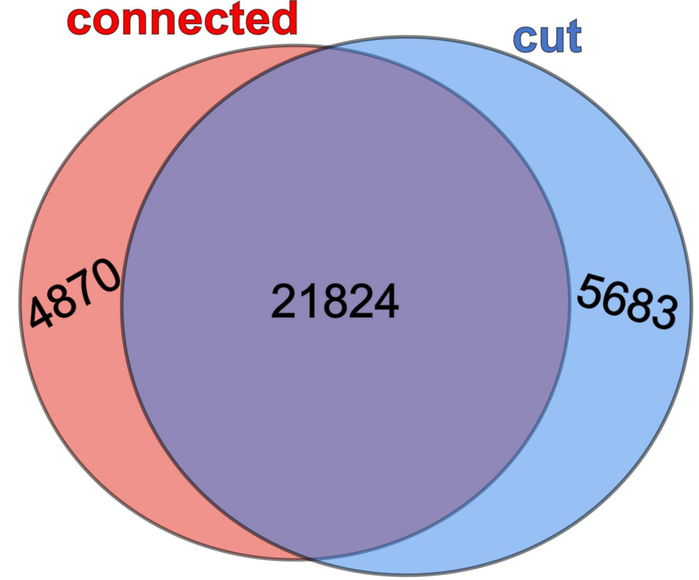

All DEGs

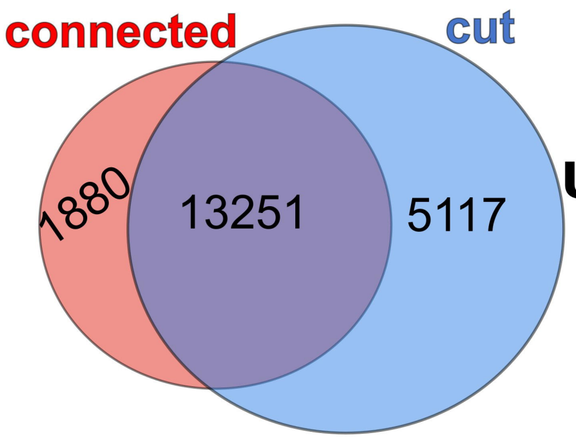

Upregulated DEGs

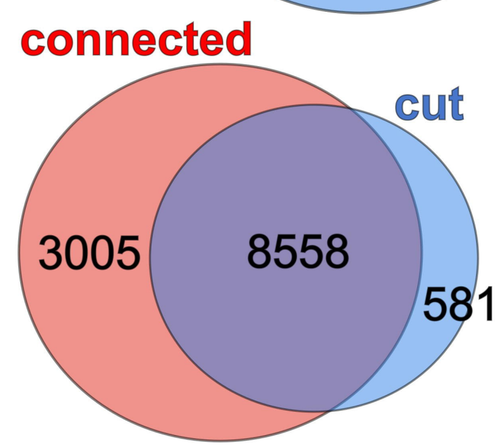

Downregulated DEGs

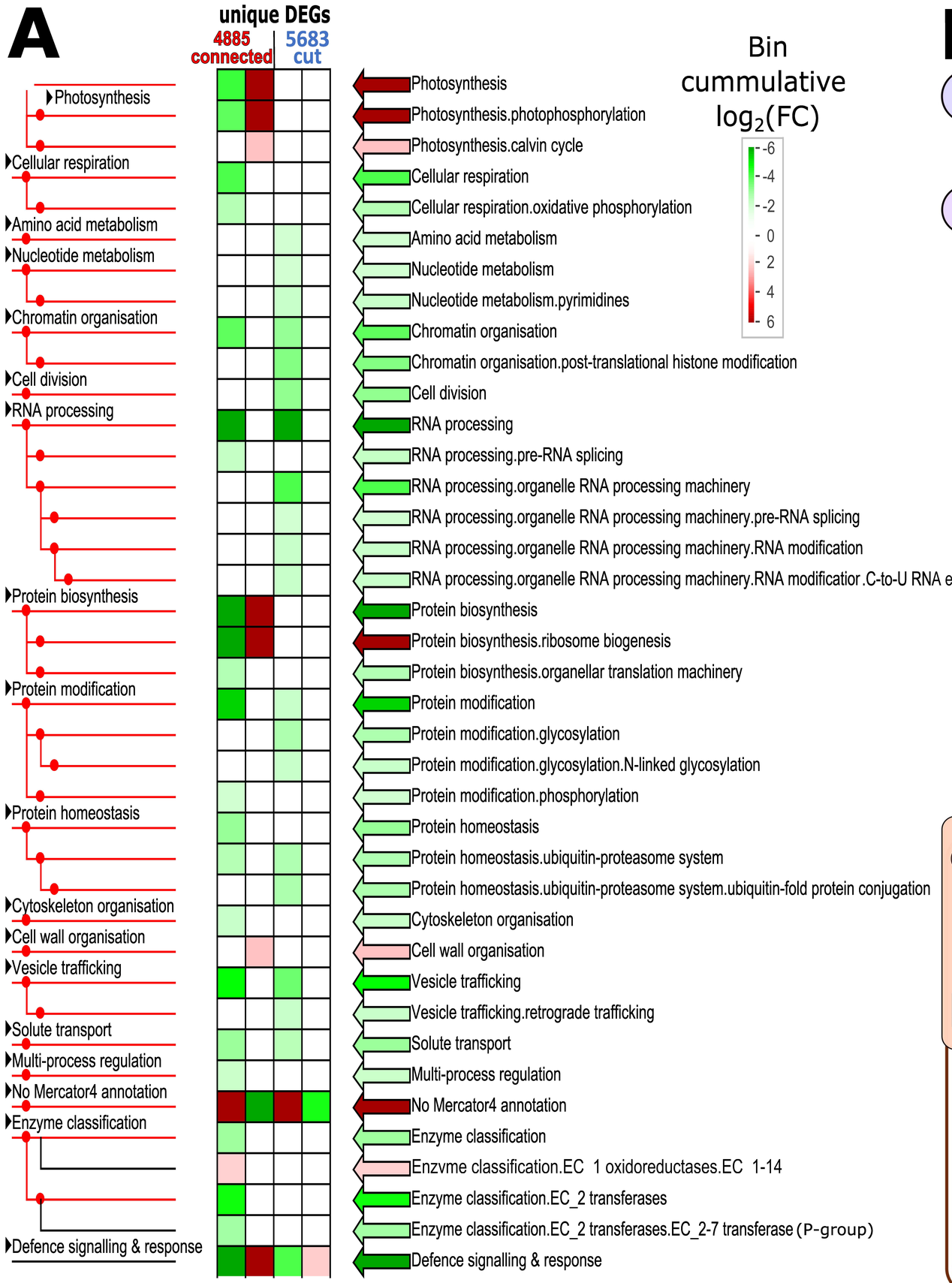
A
unique DEGs
4885 connected
5683 cut
Bin cummulative log2(FC)
-6
-4
-2
0
2
4
6
Photosynthesis
Cellular respiration
Amino acid metabolism
Nucleotide metabolism
Chromatin organisation
Cell division
RNA processing
Protein biosynthesis
Protein modification
Protein homeostasis
Cytoskeleton organisation
Cell wall organisation
Vesicle trafficking
Solute transport
Multi-process regulation
No Mercator4 annotation
Enzyme classification
Defence signalling & response
Photosynthesis
Photosynthesis.photophosphorylation
Photosynthesis.calvin cycle
Cellular respiration
Cellular respiration.oxidative phosphorylation
Amino acid metabolism
Nucleotide metabolism
Nucleotide metabolism.pyrimidines
Chromatin organisation
Chromatin organisation.post-translational histone modification
Cell division
RNA processing
RNA processing.pre-RNA splicing
RNA processing.organelle RNA processing machinery
RNA processing.organelle RNA processing machinery.pre-RNA splicing
RNA processing.organelle RNA processing machinery.RNA modification
RNA processing.organelle RNA processing machinery.RNA modificatior.C-to-U RNA editing
Protein biosynthesis
Protein biosynthesis.ribosome biogenesis
Protein biosynthesis.organellar translation machinery
Protein modification
Protein modification.glycosylation
Protein modification.glycosylation.N-linked glycosylation
Protein modification.phosphorylation
Protein homeostasis
Protein homeostasis.ubiquitin-proteasome system
Protein homeostasis.ubiquitin-proteasome system.ubiquitin-fold protein conjugation
Cytoskeleton organisation
Cell wall organisation
Vesicle trafficking
Vesicle trafficking.retrograde trafficking
Solute transport
Multi-process regulation
No Mercator4 annotation
Enzyme classification
Enzvme classification.EC 1 oxidoreductases.EC 1-14
Enzyme classification.EC_2 transferases
Enzyme classification.EC_2 transferases.EC_2-7 transferase (P-group)
Defence signalling & response

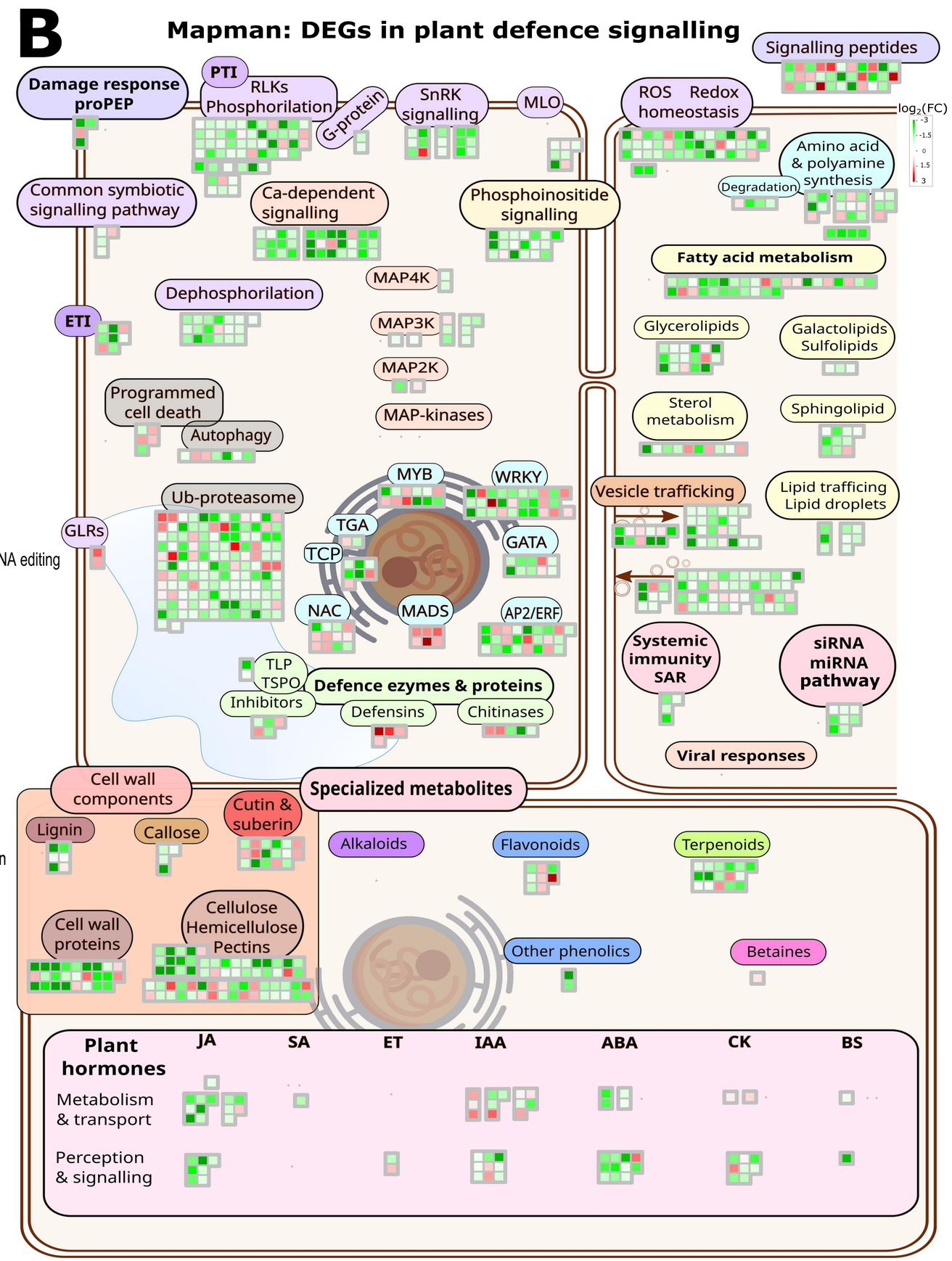
B
Mapman: DEGs in plant defence signalling
Signalling peptides
Damage response proPEP
PTI
RLKs Phosphorilation
G-protein
SnRK signalling
MLO
ROS Redox homeostasis
log2(FC)
Amino acid & polyamine synthesis
Degradation
Common symbiotic signalling pathway
Ca-dependent signalling
Phosphoinositide signalling
Fatty acid metabolism
MAP4K
Dephosphorilation
ETI
MAP3K
Glycerolipids
Galactolipids Sulfolipids
MAP2K
Programmed cell death
MAP-kinases
Sterol metabolism
Sphingolipid
Autophagy
MYB
WRKY
Vesicle trafficking
Lipid trafficking Lipid droplets
Ub-proteasome
GLRs
TGA
TCP
GATA
NAC
MADS
AP2/ERF
Systemic immunity SAR
siRNA miRNA pathway
TLP TSPO
Defence ezymes & proteins
Inhibitors
Defensins
Chitinases
Viral responses
Cell wall components
Specialized metabolites
Lignin
Callose
Cutin & suberin
Alkaloids
Flavonoids
Terpenoids
Cellulose Hemicellulose Pectins
Cell wall proteins
Other phenolics
Betaines
Plant hormones
JA
SA
ET
IAA
ABA
CK
BS
Metabolism & transport
Perception & signalling

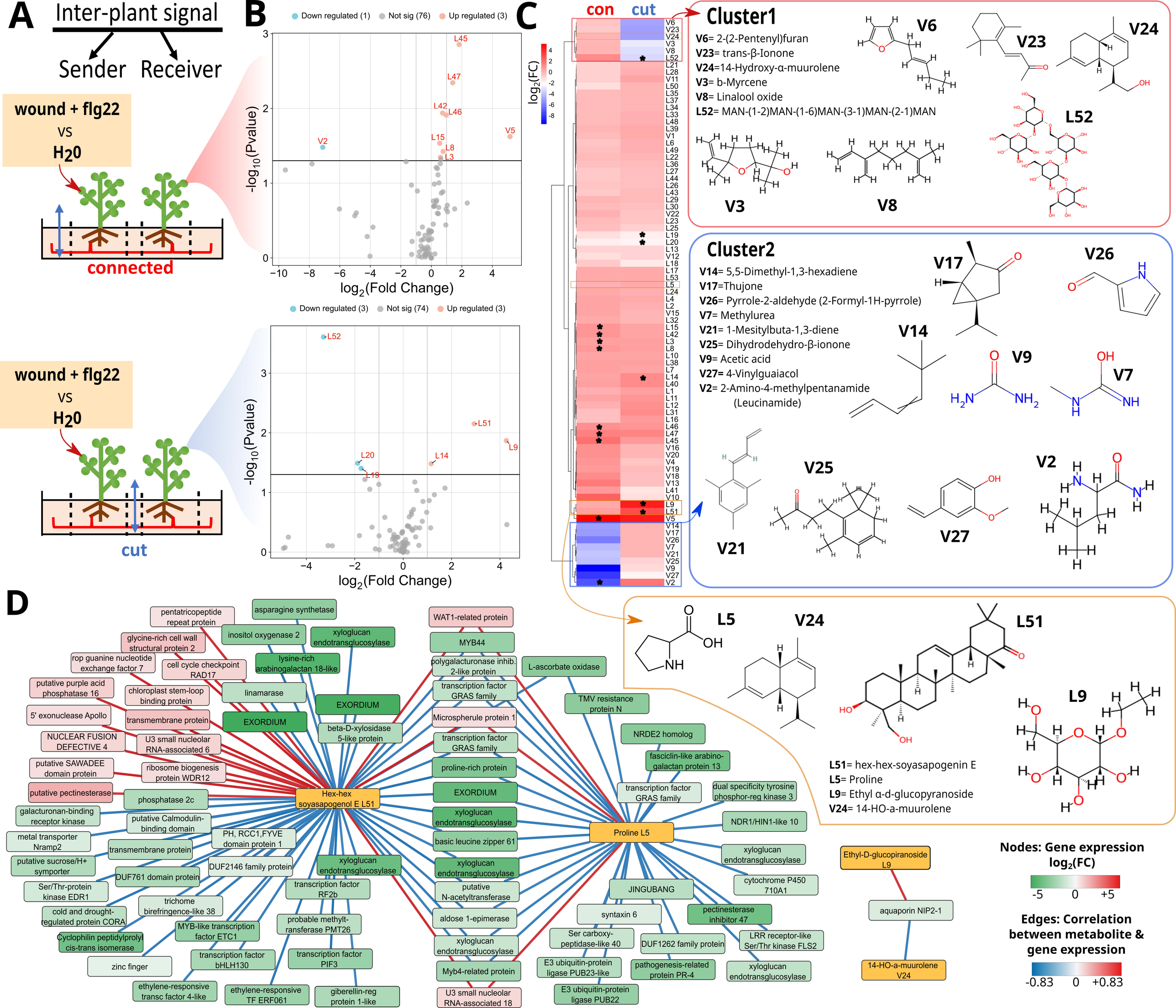
A
Inter-plant signal
Sender
Receiver
wound + flg22
VS
H20
connected
wound + flg22
VS
H20
cut
B
Down regulated (1)
Not sig (76)
Up regulated (3)
-log10(Pvalue)
log2(Fold Change)
L45
L47
L42
L46
V5
V2
L15
L8
L3
Down regulated (3)
Not sig (74)
Up regulated (3)
L52
L51
L9
L20
L19
L14
C
con
cut
log2(FC)
Cluster1
V6= 2-(2-Pentenyl)furan
V23= trans-β-Ionone
V24=14-Hydroxy-α-muurolene
V3= b-Myrcene
V8= Linalool oxide
L52= MAN-(1-2)MAN-(1-6)MAN-(3-1)MAN-(2-1)MAN
V6
V23
V24
L52
V3
V8
Cluster2
V14= 5,5-Dimethyl-1,3-hexadiene
V17=Thujone
V26= Pyrrole-2-aldehyde (2-Formyl-1H-pyrrole)
V7= Methylurea
V21= 1-Mesitylbuta-1,3-diene
V25= Dihydrodehydro-β-ionone
V9= Acetic acid
V27= 4-Vinylguaiacol
V2= 2-Amino-4-methylpentanamide
(Leucinamide)
V17
V26
V14
V9
V7
V25
V2
V21
V27
L5
V24
L51
L9
L51= hex-hex-soyasapogenin E
L5= Proline
L9= Ethyl α-d-glucopyranoside
V24= 14-HO-a-muurolene
D
pentatricopeptide repeat protein
asparagine synthetase
inositol oxygenase 2
xyloglucan endotransglucosylase
glycine-rich cell wall structural protein 2
rop guanine nucleotide exchange factor 7
cell cycle checkpoint RAD17
lysine-rich arabinogalactan 18-like
putative purple acid phosphatase 16
chloroplast stem-loop binding protein
linamarase
EXORDIUM
5' exonuclease Apollo
transmembrane protein
EXORDIUM
beta-D-xylosidase 5-like protein
NUCLEAR FUSION DEFECTIVE 4
U3 small nucleolar RNA-associated 6
putative SAWADEE domain protein
ribosome biogenesis protein WDR12
putative pectinesterase
phosphatase 2c
galacturonan-binding receptor kinase
putative Calmodulin-binding domain
metal transporter Nramp2
PH, RCC1,FYVE domain protein 1
transmembrane protein
putative sucrose/H+ symporter
DUF2146 family protein
xyloglucan endotransglucosylase
DUF761 domain protein
Ser/Thr-protein kinase EDR1
transcription factor RF2b
trichome birefringence-like 38
cold and drought-regulated protein CORA
probable methylt-ransferase PMT26
MYB-like transcription factor ETC1
Cyclophilin peptidylprolyl cis-trans isomerase
transcription factor bHLH130
transcription factor PIF3
zinc finger
ethylene-responsive transc factor 4-like
ethylene-responsive TF ERF061
giberellin-reg protein 1-like
Hex-hex soyasapogenol E L51
WAT1-related protein
MYB44
polygalacturonase inhib. 2-like protein
L-ascorbate oxidase
transcription factor GRAS family
TMV resistance protein N
Microspherule protein 1
transcription factor GRAS family
NRDE2 homolog
proline-rich protein
fasciclin-like arabino-galactan protein 13
EXORDIUM
transcription factor GRAS family
dual specificity tyrosine phosphor-reg kinase 3
xyloglucan endotransglucosylase
NDR1/HIN1-like 10
basic leucine zipper 61
Proline L5
xyloglucan endotransglucosylase
xyloglucan endotransglucosylase
cytochrome P450 710A1
putative N-acetyltransferase
JINGUBANG
aldose 1-epimerase
syntaxin 6
pectinesterase inhibitor 47
xyloglucan endotransglucosylase
Ser carboxy-peptidase-like 40
DUF1262 family protein
LRR receptor-like Ser/Thr kinase FLS2
Myb4-related protein
E3 ubiquitin-protein ligase PUB23-like
pathogenesis-related protein PR-4
xyloglucan endotransglucosylase
U3 small nucleolar RNA-associated 18
E3 ubiquitin-protein ligase PUB22
Ethyl-D-glucopiranoside L9
aquaporin NIP2-1
14-HO-a-muurolene V24
Nodes: Gene expression log2(FC)
-5
0
+5
Edges: Correlation between metabolite & gene expression
-0.83
0
+0.83

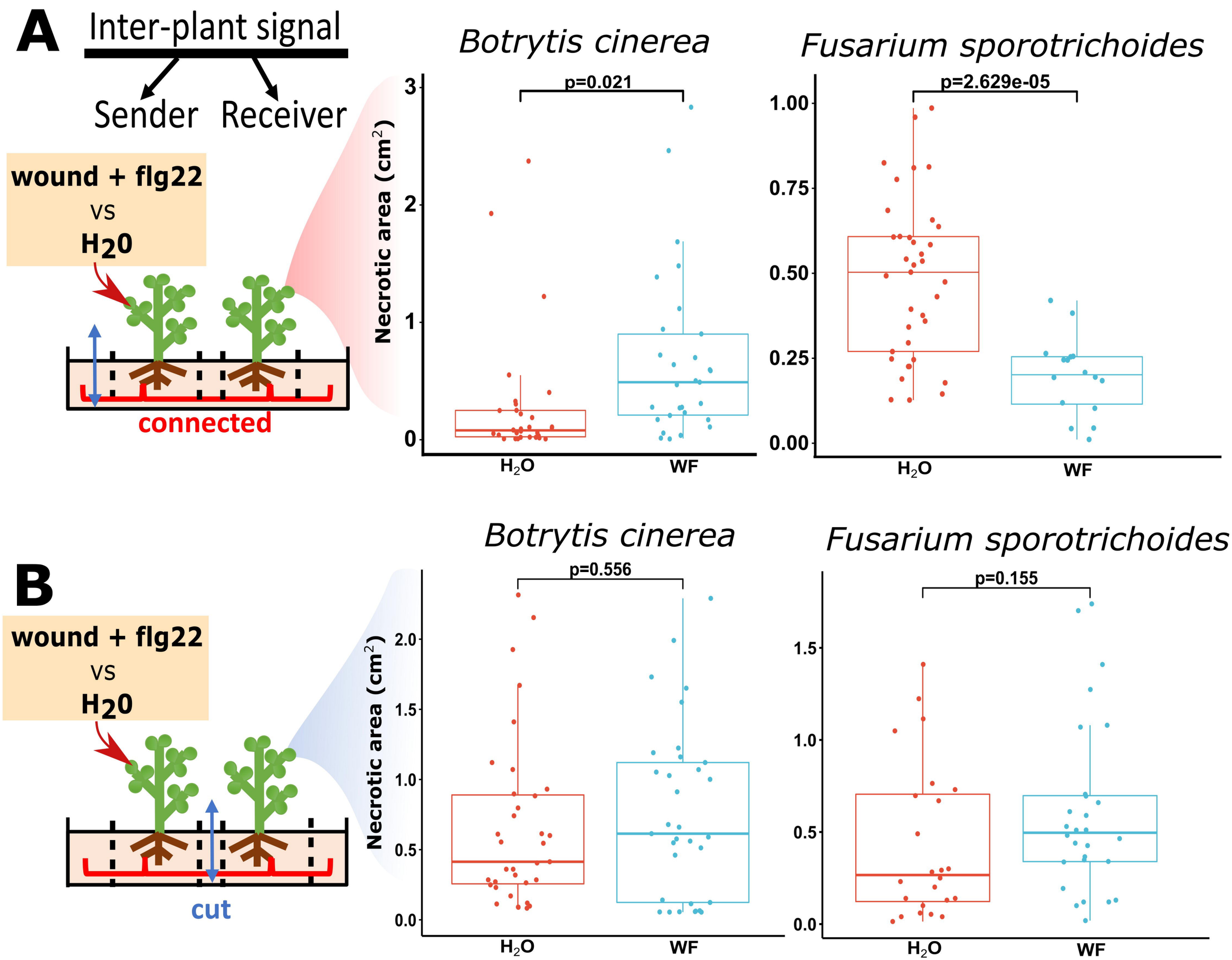
A
Inter-plant signal
Sender
Receiver
wound + flg22
vs
H20
connected
Botrytis cinerea
p=0.021
Necrotic area (cm2)
H2O
WF
Fusarium sporotrichoides
p=2.629e-05
B
wound + flg22
vs
H20
cut
Botrytis cinerea
p=0.556
Necrotic area (cm2)
H2O
WF
Fusarium sporotrichoides
p=0.155
H2O
WF